Journal of Physics D: Applied Physics

PAPER

Anomalous diffusion, nonergodicity, and ageing for exponentially and logarithmically time-dependent diffusivity: striking differences for massive versus massless particles

To cite this article: Andrey G Cherstvy *et al* 2021 *J. Phys. D: Appl. Phys.* **54** 195401

View the article online for updates and enhancements.

IOP ebooks™

Bringing together innovative digital publishing with leading authors from the global scientific community.

Start exploring the collection–download the first chapter of every title for free.

This content was downloaded from IP address 79.202.48.167 on 24/02/2021 at 16:25

IOP Publishing Journal of Physics D: Applied Physics

J. Phys. D: Appl. Phys. **54** (2021) 195401 (18pp) https://doi.org/10.1088/1361-6463/abdff0

Anomalous diffusion, nonergodicity, and ageing for exponentially and logarithmically time-dependent diffusivity: striking differences for massive versus massless particles

Andrey G Cherstvy[1,3], **Hadiseh Safdari**[2] **and Ralf Metzler**[1]

[1] Institute for Physics & Astronomy, University of Potsdam, 14476 Potsdam-Golm, Germany
[2] Max-Planck Institute for Intelligent Systems, 72076 Tübingen, Germany
[3] Institut für Physik, Humboldt-Universität zu Berlin, 12489 Berlin, Germany

E-mail: a.cherstvy@gmail.com, safdarihadiseh@gmail.com and rmetzler@uni-potsdam.de

Received 13 August 2020, revised 29 December 2020
Accepted for publication 26 January 2021
Published 25 February 2021

Abstract

We investigate a diffusion process with a time-dependent diffusion coefficient, both exponentially increasing and decreasing in time, $D(t) = D_0 e^{\pm 2\alpha t}$. For this (hypothetical) nonstationary diffusion process we compute—both analytically and from extensive stochastic simulations—the behavior of the ensemble- and time-averaged mean-squared displacements (MSDs) of the particles, both in the over- and underdamped limits. Simple asymptotic relations derived for the short- and long-time behaviors are shown to be in excellent agreement with the results of simulations. The diffusive characteristics in the presence of ageing are also considered, with dramatic differences of the over- versus underdamped regime. Our results for $D(t) = D_0 e^{\pm 2\alpha t}$ extend and generalize the class of diffusive systems obeying scaled Brownian motion featuring a power-law-like variation of the diffusivity with time, $D(t) \sim t^{\alpha-1}$. We also examine the logarithmically increasing diffusivity, $D(t) = D_0 \log[t/\tau_0]$, as another fundamental functional dependence (in addition to the power-law and exponential) and as an example of diffusivity slowly varying in time. One of the main conclusions is that the behavior of the massive particles is predominantly ergodic, while weak ergodicity breaking is repeatedly found for the time-dependent diffusion of the massless particles at short times. The latter manifests itself in the nonequivalence of the (both nonaged and aged) MSD and the mean time-averaged MSD. The current findings are potentially applicable to a class of physical systems out of thermal equilibrium where a rapid increase or decrease of the particles' diffusivity is inherently realized. One biological system potentially featuring all three types of time-dependent diffusion (power-law-like, exponential, and logarithmic) is water diffusion in the brain tissues, as we thoroughly discuss in the end.

Supplementary material for this article is available online

Keywords: anomalous diffusion, scaled Brownian motion, stochastic processes, nonstationary diffusivity, water diffusion in the brain, nonergodicity

(Some figures may appear in colour only in the online journal)

 © 2021 IOP Publishing Ltd Printed in the UK

1. Introduction

1.1. Anomalous diffusion and its models

Brownian motion (BM) features a linear spreading dynamics of the particles and a Gaussian distribution of their increments. Physical processes with non-Brownian spreading dynamics of the particles feature a nonlinear growth of the ensemble-averaged mean-squared displacement (MSD) [1–13]. In one spatial dimension, the MSD for anomalous-diffusion processes obeys a power law

$$\left\langle x^2(t)\right\rangle = \int_{-\infty}^{\infty} x^2 P(x,t)dx = 2K_\beta t^\beta, \tag{1}$$

where $P(x,t)$ is the probability density function, β is the anomalous scaling exponent, and K_β is the generalized diffusion coefficient (with the physical dimensions $[K_\beta] = \mathrm{m}^2/\mathrm{s}^\beta$). A variety of theoretical models of stochastic processes featuring the nonlinear MSD growth (1) has emerged in the last decades [5, 7, 10, 13] targeting the underlying physical mechanisms and offering the mathematical description for many experimental and simulations-based observations of anomalous diffusion (often transient). The list is by now too long to adequately overview all evidence and length/time scales here. From the biological perspective, for instance, we mention a number of real systems and models of anomalous diffusion, including those in living cells, on lipid membranes, and in artificially crowded media [10–61].

Recently, a number of diffusion models of continuous-time random walk type [62–73], viscoelastic diffusion [10, 74–76], fractional BM [5, 77–80], some combinations of continuous-time random walk and fractional BM [81–83], diffusion based on the fractional Langevin equation [10, 84], heterogeneous diffusion processes with the space-dependent diffusivity [85–94] $D(x) \sim |x|^\epsilon$ yielding the MSD $\left\langle x^2(t)\right\rangle \sim t^{\frac{2}{2-\epsilon}}$ (see also the infinite ergodic theory for such $D(x)$ forms [95], combinations of $D(x) \sim |x|^\epsilon$ with fractional BM [96], with multiplicative-noise [97] processes for colored Gaussian [98] and Lévy noise [99], diffusion in heterogeneous velocity fields [100], with potential fields [101] as well as $D(x)$-diffusion in comb and fractal structures [102]). The diffusive and nonergodic properties of heterogeneous systems with exponential $D(x)$ were also considered [89]. Both under- and overdamped BM at nonhomogeneous temperature coupled to the diffusivity were studied [103].

As more examples, the spreading dynamics in crowded and heterogeneous environments [13, 39, 60, 73, 104–113], diffusion with systematically varying time-dependent diffusivities $D(t)$ [114–123] (including the dynamics of granular matter slowing down due to inelastic collisions [119, 124], slowing down $D(t)$-dependent diffusion in brain tissues [125–133] (see also [134] and the magnetic-resonance-imaging-studies of diffusion in general [135, 136]) were examined. The particle-spreading dynamics in time- and space-fluctuating-diffusivity landscapes [46, 137–143], in expanding/contracting media [144, 145], and in the models with diffusing, switching and random diffusivities (including superstatistical ones) [60, 76, 112, 140, 146–152] was studied as well.

A number of single-trajectory-based algorithms of assessment-and-ranking and parameter-estimation of realizable models of diffusion for a data set of tracer positions (as recorded in single-particle-tracking experiments [153–156]) were developed [51, 142, 157–162]. This list includes the recent Bayesian-statistics-based methods [51, 142, 163, 165], machine-learning approaches [83, 159, 166–171], concepts of recurrent neural networks [162], inference-based methods [158, 161] and the spectral-density single-trajectory analysis [160]. We mention here the models with 'switching' between different types of (anomalous) diffusion (intermittent processes) [60, 124, 147, 161, 162, 164, 172–175]. The importance of particle-localization errors onto determination of 'apparent' subdiffusion [176–181] should also be emphasized (see also the recent studies on quantifying error corrections in particle-tracking microrheology [182] and for ergodic ensembles of colloidal particles [183]). Recent applications of anomalous diffusion and nonergodicity [185–189] for the analysis of income growth in gambling are also to be mentioned [190]. Finally, for a perspective on nonergodicity and possible sources of bias in biological, biomedical, behavioral, and psychological systems we refer to [191].

1.2. Time-dependent diffusivity

For the time-dependent diffusivity of the form

$$D(t) \sim t^{\beta-1} \tag{2}$$

the process of so called scaled BM (SBM) is realized, with

$$\left\langle x^2(t)\right\rangle = 2D(t)t \simeq t^\beta, \tag{3}$$

studied in depth both in the over- and underdamped limits [93, 116–118, 121, 122, 139] as well as recently in the presence of resetting [123]. The special case of SBM yielding ultraslow diffusion with the log-like MSD growth was considered too [120]. We refer here also to the recent review on ultraslow diffusion in heterogeneous materials [199]. Experimentally, the models of power-law $D(t)$ were utilized recently, e.g. to rationalize water diffusion in brain tissues [130, 131].

The current study unveils the ensemble- and time-averaged particle displacements and the spreading characteristics of a Markovian yet nonstationary stochastic process with a time-dependent diffusivity. As the time-domain analogy of the modification of heterogeneous diffusion processes $D(x) \sim |x|^\epsilon$ to exponentially and logarithmically position-varying diffusivity [89], $D(x) \sim e^{-x}$ and $D(x) \sim \log x$, we here extend the framework of the canonical SBM model to the diffusivity exponentially and logarithmically varying in time. Specifically, we consider both increasing and decreasing diffusivities,

$$D(t) = D_0 e^{\pm 2\alpha t}, \tag{4}$$

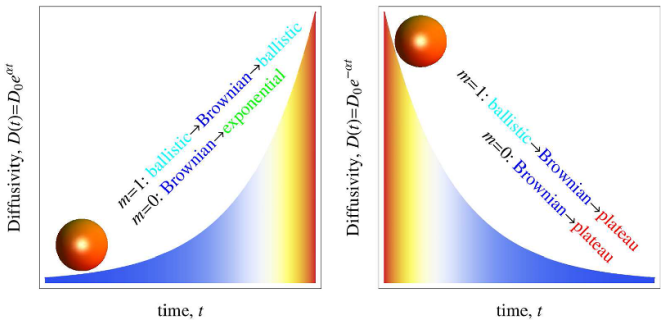

Figure 1. Schematic representation of the dynamics of *massive* ($m=1$) and *massless* ($m=0$) particles with diffusivities varying exponentially in time. The predicted transitions in the regimes of MSD growth are indicated, see also table 1.

and call this process exponential SBM (ESBM), see the schematic in figure 1, as well as the scenario with

$$D(t) = D_0 \log[t/\tau_0] \tag{5}$$

called below logarithmic SBM (LSBM). We refer to [192] for an example of logarithmically slow dynamics[3].

We investigate the short- and long-time scaling behavior for the MSD (1) and the time-averaged MSD (TAMSD) defined in equation (7) below both for under- and overdamped motion. The aspects of ageing for $D(t)$ of the form (2) were examined analytically and by simulations in [122] using the MSD, the TAMSD, and the ergodicity breaking parameter (denoted below as EB) and we generalize this approach to (4) and (5) here. We uncover the properties of aged ESBM below as well.

We consider the spreading dynamics of particles with $D(t)$ of the form (4), with the time-local fluctuation-dissipation relation [97, 103, 115] assumed to hold. Thus, time variations of the temperature $\mathcal{T}(t)$ and diffusivity $D(t)$ are coupled to that of the friction coefficient $\gamma(t)$ of the particle of mass m via

$$D(t) = k_B \mathcal{T}(t)/[m\gamma(t)], \tag{6}$$

where k_B is the Boltzmann constant. This condition of the local thermal equilibrium implies that the internal relaxation in the system occurs on time scales much shorter than a typical time scale of temperature variation.

1.3. Structure of the paper

The paper is organized as follows. In section 2 we present the Langevin equation in the underdamped limit for $D(t) = D_0e^{2\alpha t}$. We describe the approximations employed and define relevant observables. In section 3.1 we present the main results for the MSD and mean TAMSD obtained from the analytic calculations and computer simulations, while the behavior of the EB parameter is considered in section 3.2. We also discuss the underlying mathematical features and physical consequences of the main findings. The main scaling relations for the MSD and TAMSD in all the scenarios are summarized in table 1. In section 4 the findings for all three scenarios ($D(t) = D_0e^{2\alpha t}$, $D(t) = D_0e^{-2\alpha t}$, and $D(t) = D_0 \log[t/\tau_0]$) are discussed and future developments of diffusion models with time-varying $D(t)$ are outlined. The details of analytical derivations and auxiliary figures are presented in Apps. A, B, and C (available online at stacks.iop.org/JPD/54/195401/mmedia). Finally, in section 5 we discuss the relevance of these non-stationary diffusion models to the description of water diffusion in gray- and white-matter tissues of the human brain. This deeply complex biological system with intricate behaviors on multiple scales serves as a motivation for the current theoretical analysis.

[3] Throughout the text, we reserve β for the MSD scaling exponent, parameter α denotes the rate of diffusivity variation for the case $D(t) \sim e^{\pm 2\alpha t}$, and τ_0 is a typical time-scale for the $D(t) \sim \log[t/\tau_0]$ scenario.

2. Physical observables and simulation scheme

2.1. MSD, TAMSD, EB parameter, and ageing

The TAMSD—the physical observable central, for instance, to quantify the dynamics in the single-particle-tracking experiments—is defined (in one spatial dimension) as [5, 10]

$$\overline{\delta^2(\Delta)} = \frac{1}{T-\Delta} \int_0^{T-\Delta} [x(t+\Delta) - x(t)]^2 \, dt. \tag{7}$$

Here Δ is the lag time (setting the averaging window along the time series) and T is the total length of the trajectory. After averaging over N statistically independent realizations of a process, the mean TAMSD at a lag time Δ is computed as

$$\left\langle \overline{\delta^2(\Delta)} \right\rangle = \frac{1}{N} \sum_{i=1}^{N} \overline{\delta_i^2(\Delta)}. \tag{8}$$

For an ergodic diffusive process, the MSD (1) and the TAMSD (7) are identical in the limit $\Delta/T \ll 1$ [5, 10]. Here, the quantitative measure of ergodicity [184–186, 189] is the EB parameter based on the fourth moment of the particle displacement [10, 62, 77],

$$\mathrm{EB}(\Delta) = \frac{\left\langle \left(\overline{\delta^2(\Delta)}\right)^2 \right\rangle - \left\langle \overline{\delta^2(\Delta)} \right\rangle^2}{\left\langle \overline{\delta^2(\Delta)} \right\rangle^2} = \left\langle \xi^2(\Delta) \right\rangle - 1. \tag{9}$$

Here, the normalized TAMSD

$$\xi(\Delta) = \overline{\delta^2(\Delta)} \Big/ \left\langle \overline{\delta^2(\Delta)} \right\rangle \tag{10}$$

quantifies relative deviations via dispersion of the distribution of individual TAMSD realizations around their mean (8) divided by the mean TAMSD squared. For an ergodic system of diffusing particles at any finite lag time Δ the relation

$$\lim_{T\to\infty} \mathrm{EB}(\Delta) \to 0 \tag{11}$$

holds and in the limit $\Delta \ll T$ each individual TAMSD realization approaches the MSD at the same (lag) time,

Table 1. Summary of the asymptotic results for the $D(t) = D_0 e^{\pm 2\alpha t}$ and $D(t) = D_0 \log[t/\tau_0]$ diffusion scenarios regarding the MSD and mean TAMSD (for the nonaged and aged conditions) at short, intermediate, and long times. The conclusion regarding WEB—the equivalence of the MSD and the TAMSD in the limit of short (lag) times and long trajectories, given by equation (12)—is provided in the last column.

Time-dependent diffusivity scenario	MSD TAMSD	Short time	Intermediate time	Long time	WEB
Massive $D(t) = D_0 e^{2\alpha t}$ nonaged	$\langle x^2(t)\rangle$ $\left\langle \overline{\delta^2(\Delta)}\right\rangle$	$\approx D_0\gamma_0 t^2$, eq. (A6) $\approx D_0\gamma_0\Delta^2$, eq. (A11)	$\approx 2D_0 t$, eq. (A8) $\approx 2D_0\Delta(1+\alpha T)$, eqs. (A12), (A14), (A15)	$\approx D_0\gamma_0 t^2$, eq. (A9) eqs. (A10), (A15)	No
Massive $D(t) = D_0 e^{2\alpha t}$ aged	$\langle x_a^2(t)\rangle$ $\left\langle \overline{\delta_a^2(\Delta)}\right\rangle$	$\approx D_0\gamma_0 t^2$, eq. (A18) $\approx D_0\gamma_0\Delta^2$, eq. (A19)	eq. (A17) eq. (A20)	eq. (A17) eqs. (A20), (A21)	No
Massless $D(t) = D_0 e^{2\alpha t}$ nonaged	$\langle x^2(t)\rangle$ $\left\langle \overline{\delta^2(\Delta)}\right\rangle$	$\approx 2D_0 t$, eq. (A25) $\approx 2D_0\Delta\frac{e^{2\alpha T}}{2\alpha T}$, eq. (A27)	$\frac{D_0}{\alpha}\left(e^{2\alpha t}-1\right)$, eq. (A23) eq. (A26)	$\approx \frac{D_0}{\alpha}e^{2\alpha t}$, eq. (A24) eqs. (A26), (A29)	Yes
Massless $D(t) = D_0 e^{2\alpha t}$ aged	$\langle x_a^2(t)\rangle$ $\left\langle \overline{\delta_a^2(\Delta)}\right\rangle$	$\approx 2D_0 t e^{2\alpha t_a}$, eq. (A30) $\approx 2D_0\Delta\frac{e^{2\alpha T}}{2\alpha T}e^{2\alpha t_a}$, eqs. (A27), (A31)	eq. (A30) eq. (A31)	eq. (A30) eq. (A31)	Yes
Massive $D(t) = D_0 e^{-2\alpha t}$ nonaged	$\langle x^2(t)\rangle$ $\left\langle \overline{\delta^2(\Delta)}\right\rangle$	$\approx D_0\gamma_0 t^2$, eq. (B3) $\approx D_0\gamma_0\Delta^2$, eq. (B8)	$\approx 2D_0 t$, eq. (B5) $\approx 2D_0\Delta(1-\alpha T)$, eqs. (B9), (B10)	$\approx \frac{D_0}{\alpha}$, eq. (B4) eq. (B10)	No
Massive $D(t) = D_0 e^{-2\alpha t}$ aged	$\langle x_a^2(t)\rangle$ $\left\langle \overline{\delta_a^2(\Delta)}\right\rangle$	$\approx D_0\gamma_0 t^2$, eq. (B12) $\approx D_0\gamma_0\Delta^2$, eq. (B15)	$\approx 2D_0 t e^{-2\alpha t_a}$, eq. (B13) eq. (B16)	$\approx \frac{D_0}{\alpha}e^{-2\alpha t_a}$, eq. (B14) eq. (B16)	No
Massless $D(t) = D_0 e^{-2\alpha t}$ nonaged	$\langle x^2(t)\rangle$ $\left\langle \overline{\delta^2(\Delta)}\right\rangle$	$\approx 2D_0 t$, eq. (B21) $\approx \frac{2D_0\Delta}{2\alpha T}$, eq. (B22)	$\frac{D_0}{\alpha}\left(1-e^{-2\alpha t}\right)$, eq. (B19) eq. (B20)	$\approx \frac{D_0}{\alpha}$, eq. (B23) $\approx \frac{D_0}{\alpha}$, eq. (B24)	Yes
Massless $D(t) = D_0 e^{-2\alpha t}$ aged	$\langle x_a^2(t)\rangle$ $\left\langle \overline{\delta_a^2(\Delta)}\right\rangle$	$\approx 2D_0 t e^{-2\alpha t_a}$, eq. (B25) $\approx \frac{2D_0\Delta}{2\alpha T}e^{-2\alpha t_a}$, eq. (B26)	eq. (B25) eq. (B26)	eq. (B25) eq. (B26)	Yes
Massive $D(t) = D_0 \log\left[\frac{t}{\tau_0}\right]$ nonaged	$\langle x^2(t)\rangle$ $\langle x^2(t)\rangle$ $\left\langle \overline{\delta^2(\Delta)}\right\rangle$	$\approx \frac{D_0\gamma_0(\Delta t)^2}{1+\gamma_0\tau_0}$, eqs. (C8) $\approx D_0\gamma_0(\Delta t)^2$, eq. (C10) $\approx D_0\gamma_0\Delta^2$, eq. (C18)	eq. (C6) eq. (C15)	$\approx 2D_0\log\left[\frac{t}{\tau_0}\right]t$, eq. (C14) $\approx 2D_0\log\left[\frac{\Delta}{\tau_0}\right]\Delta$, eq. (C20)	Yes No
Massive $D(t) = D_0 \log\left[\frac{t}{\tau_0}\right]$ aged	$\langle x_a^2(t)\rangle$ $\left\langle \overline{\delta_a^2(\Delta)}\right\rangle$	$\approx \frac{D_0\gamma_0 t^2}{1+\gamma_0\tau_0}$, eq. (C22) $\approx D_0\gamma_0 t^2$, eq. (C23) $\approx D_0\gamma_0\Delta^2$, eq. (C29)	eq. (C26) eq. (C30)	$\approx 2D_0\log\left[\frac{t}{\tau_0}\right]t$, eq. (C26) eq. (C30)	Yes No
Massless $D(t) = D_0 \log\left[\frac{t}{\tau_0}\right]$ nonaged	$\langle x^2(t)\rangle$ $\left\langle \overline{\delta^2(\Delta)}\right\rangle$	$\approx \frac{D_0(t-t_0)^2}{\tau_0}$, eq. (C32) $\approx 2D_0\log\left[\frac{T}{\tau_0}\right]\Delta$, eq. (C36)	eq. (C31) eq. (C36)	$\approx 2D_0\log\left[\frac{t}{\tau_0}\right]t$, eq. (C33) eq. (C35)	Yes
Massless $D(t) = D_0 \log\left[\frac{t}{\tau_0}\right]$ aged	$\langle x_a^2(t)\rangle$ $\left\langle \overline{\delta_a^2(\Delta)}\right\rangle$	$\approx \frac{D_0(t-t_0)^2}{\tau_0}\frac{\log\left[\frac{t_a}{\tau_0}\right]}{\log\left[\frac{t}{\tau_0}\right]}$, eq. (C40) $\approx 2D_0\log\left[\frac{T}{\tau_0}\right]\Delta^{\frac{\log[t_a/\tau_0]}{\log[T/\tau_0]}}$, eq. (C41)	eq. (C38) eq. (C39)	eq. (C38) eq. (C39)	Yes

$$\overline{\delta^2(\Delta)} \to \langle x^2(\Delta)\rangle. \tag{12}$$

This definition of ergodicity in the Khinchin–Boltzmann sense is less strict than the classical 'mixing' definition [6, 185, 193]. The latter implies exponential divergence of trajectories with the same starting point in phase-space[4].

For ESBM with

$$D(t) = D_0 e^{2\alpha t} \tag{13}$$

we solve the stochastic Langevin equation for the massive ($m = 1$) and massless potential-free particles [119–122],

$$m\frac{d^2x(t)}{dt^2} + \gamma(t)\frac{dx(t)}{dt} = \sqrt{2D(t)}\gamma(t)\eta(t). \tag{14}$$

This system is driven by the Gaussian noise $\eta(t)$ with zero mean $\langle\eta(t)\rangle = 0$ and unit variance

$$\langle\eta(t)\eta(t')\rangle = \delta(t-t'). \tag{15}$$

The friction coefficient is set to depend on time as

$$\gamma(t) = \gamma_0 e^{-2\alpha t} \tag{16}$$

and the temperature is set to be constant,

$$\mathcal{T}(t) = \mathcal{T}_0, \tag{17}$$

in order to satisfy relation (6). Note also that a model with a time-dependent temperature and different dependence of friction on time is also possible for the diffusivity (13) with condition (6) still satisfied.

[4] The general definition of ergodicity based on a metric for any physical observable was employed already by Mountain and Thirumalai [194–196] (and introduced even earlier in [197]). To recapitulate the main conclusions, the 'order parameter' Ω similar to EB (9) was used [194–196] as a quantitative measure of sampling of the configuration space by the particles and of the related (non)-ergodicity (applied, e.g. to supercooled liquids and binary mixtures of soft interacting spheres). For the energy-fluctuation metric, e.g. the definition was based on the total energies of the particles E_i averaged over the trajectory length T, namely

$$\overline{E_i(T)} = \frac{1}{T}\int_0^T E_i(s)ds. \tag{38}$$

For a finite classical system of N particles with conservative forces, the energy-related ergodicity parameter was defined as the ensemble-average [194–196],

$$\Omega_{\overline{E}}(T) = \frac{1}{N}\sum_{i=1}^{N}\left[\overline{E_i(T)} - \frac{1}{N}\sum_{j=1}^{N}\overline{E_j(T)}\right]^2. \tag{39}$$

This quantity vanishes for an 'effectively ergodic' [198] dynamics at finite observation times T [194–196] provided the time-scale of internal relaxation or dynamics is $\tau_{\rm int} \ll T$. The rate of exploration of the configurational space and of the convergence to ergodicity is given by the 'diffusion constant', $D_{\overline{E}}$, with the fundamental decay law with the trajectory length T given as

$$\Omega_{\overline{E}}(T)/\Omega_{\overline{E}}(0) \sim 1/(D_{\overline{E}}T). \tag{40}$$

The typical 'mixing time', $\tau_{\rm mix}$, depends on the temperature $\mathcal{T}$ of the system via $D_{\overline{E}}$ as follows [194–196] $\tau_{\rm mix}(\mathcal{T}) \sim 1/D_{\overline{E}}(\mathcal{T})$.

From the velocity–velocity correlation function, $\langle v(t_1)v(t_2)\rangle$, the MSD and the mean TAMSD are expressed as [7]

$$\langle x^2(t)\rangle = 2\int_0^t dt_1\int_{t_1}^t dt_2\,\langle v(t_1)v(t_2)\rangle \tag{18}$$

and

$$\left\langle\overline{\delta^2(\Delta)}\right\rangle = \frac{\int_0^{T-\Delta} dt\left[\langle x^2(t+\Delta)\rangle - \langle x^2(t)\rangle - 2A(t,\Delta)\right]}{T-\Delta}, \tag{19}$$

respectively, where we defined [121]

$$A(t,\Delta) = \int_0^t dt_1\int_t^{t+\Delta} dt_2\,\langle v(t_1)v(t_2)\rangle. \tag{20}$$

In the presence of ageing—when the recording of the time series starts after a given time t_a after the preparation of a system—the aged MSD and aged TAMSD are given by, correspondingly [7, 10, 122],

$$\langle x_a^2(t)\rangle = 2\int_{t_a}^{t_a+t} dt_1\int_{t_1}^{t_a+t} dt_2\,\langle v(t_1)v(t_2)\rangle \tag{21}$$

and

$$\overline{\delta_a^2(\Delta)} = \frac{1}{T-\Delta}\int_{t_a}^{t_a+T-\Delta}\left[x(t+\Delta)-x(t)\right]^2 dt. \tag{22}$$

The correlator $\langle v(t_1)v(t_2)\rangle$ used in (21) is nonaged [122].

2.2. Discretization scheme

After the discretization of the trajectory into $T/\delta t$ steps, in the computer algorithm the time-step of integration was set to $\delta t = 1$ (unless explicitly specified otherwise). Thus, at a time instance t_{n+1} the following discrete forward-type Itô's scheme for the velocity and position of the particle is solved,

$$\begin{aligned} v(t_{n+1}) = v(t_n) &+ \sqrt{2D(t_n)}\gamma(t_n)\eta(t_n)\sqrt{t_{n+1}-t_n} \\ &- \gamma(t_n)v(t_n)(t_{n+1}-t_n), \end{aligned} \tag{23}$$

and

$$x(t_{n+1}) = x(t_n) + v(t_n)(t_{n+1}-t_n). \tag{24}$$

Below, we present the results in terms of the dimensionless displacements and time; the values of the model parameters (D_0, α, γ_0, T, etc) are also given in the figure captions without their physical units (for simplicity).

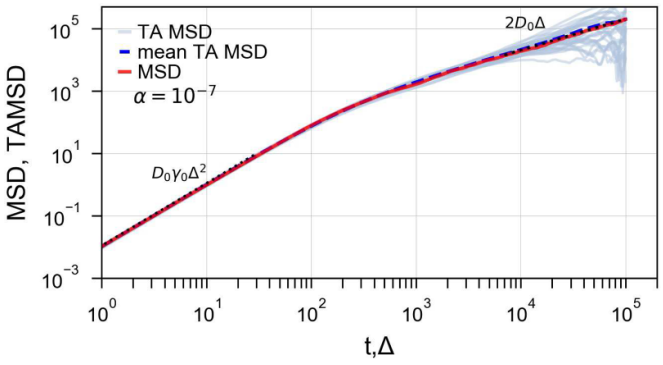

Figure 2. MSD, mean TAMSD, and the spread of individual TAMSD trajectories for the *massive* particles with $D(t) = D_0 e^{2\alpha t}$. The ballistic asymptote (A6) and the linear asymptote (A8) are the dashed lines at short and intermediate-to-long times, correspondingly. Parameters: $m = 1$, $D_0 = 1$, $\gamma_0 = 10^{-2}$, $\alpha = 10^{-7}$, $T = 10^5$. MSD involves averaging over $N = 500$ time series, while $N = 30$ TAMSD trajectories are shown in the plot to visualize the degree of their spread.

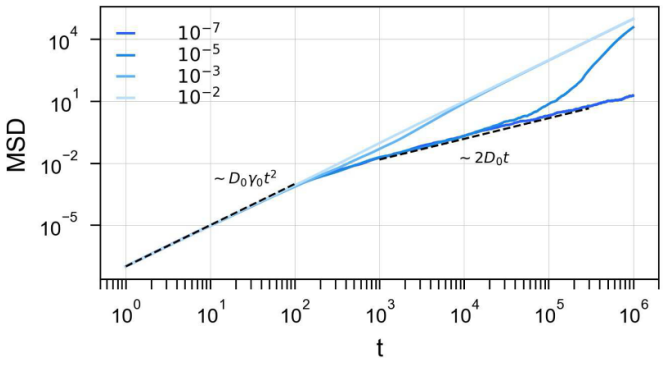

Figure 3. Ballistic-to-linear and linear-to-ballistic transitions in the MSD growth for the *massive* particles with $D(t) = D_0 e^{2\alpha t}$, as obtained from computer simulations for varying α values (as specified in the legend, $\alpha = 10^{-7}, 10^{-5}, 10^{-3}, 10^{-2}$). The asymptotes (A6) and (A8) are the dashed lines. Parameters: $m = 1$, $D_0 = 10^{-5}$, $\gamma_0 = 10^{-2}$, $T = 10^6$, $N = 200$.

3. Main results for $D(t) = D_0 e^{2\alpha t}$

In the main text, for the MSD and TAMSD we present the key results of analytical calculations and computer simulations for $D(t) = D_0 e^{2\alpha t}$ (sections 3.1 and 3.2). The detailed derivations for rapidly varying diffusivities $D(t) = D_0 e^{2\alpha t}$ and $D(t) = D_0 e^{-2\alpha t}$ as well as for a slowly varying form $D(t) = D_0 \log[t/\tau_0]$ are given in Apps. A, B, and C, correspondingly (together with supplementary figures for ESBM and LSBM).

3.1. MSD and mean TAMSD for $D(t) = D_0 e^{2\alpha t}$

3.1.1. Massive particles. In figure 2 the particle displacements in the underdamped limit are shown. Both the MSD and mean TAMSD for the *massive* particles start ballistically with time, consistent with the theoretical predictions of equations (A6) and (A11). The variation of the MSD and the mean TAMSD with α is presented in figures 3 and AA1, respectively. At moderate values of α for intermediate lag times—roughly, from a characteristic time $\sim 1/\gamma_0$ of momentum relaxation to the diffusivity-variation time $\sim 1/\alpha$—a region of linear growth of $\langle x^2(t)\rangle$ and $\left\langle \overline{\delta^2(\Delta)} \right\rangle$ is observed, consistent with the analytical predictions (A8) and (A12), respectively.

At long times the MSD is ballistic again, in agreement with (A9), see figures 2 and 3. We find that for very small α values, such that $\alpha T \ll 1$ and almost no implications of the time-dependent diffusivity effectively present, the mean TAMSD starts ballistically following $\approx D_0\gamma_0\Delta^2$, as equation (A11) predicts, while at intermediate and long times the standard diffusion law

$$\left\langle \overline{\delta^2(\Delta)} \right\rangle \approx 2D_0\Delta \tag{25}$$

is detected. For larger values of the parameter α, such that $\alpha T \gg 1$, in the entire region of lag times a ballistic growth of the TAMSD is observed, see figure AA1. Under these conditions, the value of the lag time from which the linear TAMSD growth is expected to occur shifts progressively toward larger values, so that they can be even larger than the total length of the trajectory investigated (see equation (A16)). In the region of time where the nonaged and aged MSDs of the massive particles with $D(t) = D_0 e^{2\alpha t}$ turn from the intermediate-time linear to the long-time ballistic growth, the MSD increases with time faster than ballistically, see figures 3, 4 and AA3(a).

Note that to observe all regimes of diffusion the trajectory should be long enough, i.e. $T \gg 1/\alpha$, whereas for rather large α values we indeed only detect the initial ballistic regime, see figure AA2. The amplitude spread of individual TAMSD realizations is found to be very small at short lag times, but increases toward the end of the trajectories, as it generally should (also for standard BM [10]). This effect is due to worsening statistics as the lag time approaches the trajectory length [10]. Note that as $\Delta \to T$ for some parameters the mean TAMSD drops in magnitude, as seen in figure AA2.

Considering the ageing dynamics of ESBM for the massive particles with $D(t) = D_0 e^{2\alpha t}$, for the aged MSD (21) we find that the time dependence of $\langle x_a^2(t)\rangle$ changes neither at short nor at long times. This is predicted theoretically (see equation (A18) and figure 4) and supported by the simulations (see figure AA3(a)). The latter also demonstrates that the regime of linear diffusion (A8) vanishes for long ageing times t_a (the limit of strong ageing). The evolution of $\langle x_a^2(t)\rangle$ for varying t_a predicted theoretically and obtained from the simulations are in excellent, quantitative agreement (when plotted for the same parameters, as in figures 4 and AA3(a)).

The behavior of the aged mean TAMSD, $\left\langle \overline{\delta_a^2(\Delta)} \right\rangle$, as obtained from our computer simulations for the massive particles with $D(t) = D_0 e^{2\alpha t}$ is presented in figures AA3(b) and AA4(a),(b). We find that for very small α values, at $\alpha T \ll 1$, the effects of ageing are almost invisible: at short lag times $\Delta \lesssim 1/\gamma_0$ the $\left\langle \overline{\delta_a^2(\Delta)} \right\rangle$ magnitude starts ballistically according to (A11) and at intermediate-to-long lag times the standard diffusion law (A12) is observed, as shown in figure

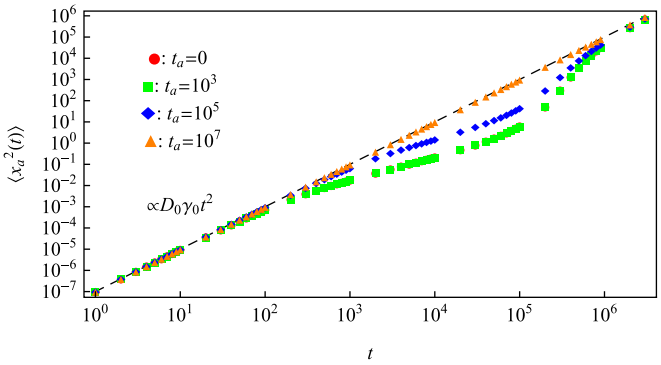

Figure 4. Aged MSD $\left\langle x_a^2(t)\right\rangle$ for $D(t)=D_0e^{2\alpha t}$ of the *massive* particles for the same parameters as in figure AA3, as obtained from the analytical expressions (A17). The dashed line is the ballistic asymptote (A18) (which describes both the short- and long-time behavior).

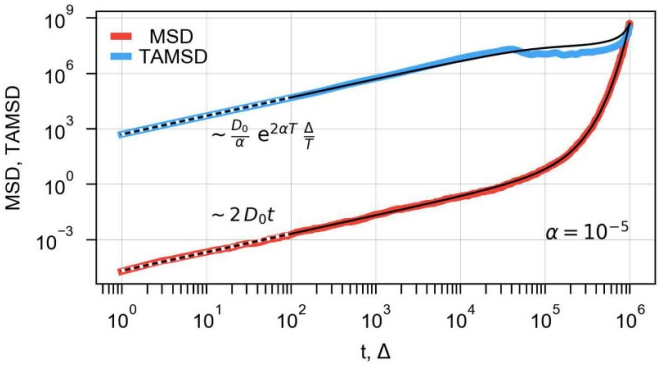

Figure 5. MSD and mean TAMSD for the overdamped ESBM (for the *massless* particles) with $D(t)=D_0e^{2\alpha t}$ obtained by computer simulations. The full theoretical predictions (A23) and (A26) are the solid black curves, while the short-time asymptotes for the MSD (A25) and mean TAMSD (A27) are shown as the white dashed lines. Parameters: $m=0$, $D_0=10^{-5}$, $\gamma_0=10^{-2}$, $\alpha=10^{-5}$, $T=10^6$, and $N=200$.

AA4(a). For larger α values the magnitude of $\left\langle\overline{\delta_a^2(\Delta)}\right\rangle$ at long times increases substantially for larger t_a values; the overall $\left\langle\overline{\delta_a^2(\Delta)}\right\rangle$ versus Δ behavior remains nearly ballistic at short times and turns linear at long lag times, see figure AA3(b). For a gradually increasing t_a value, the threshold lag-time value $\Delta^\star$ after which the linear regime of the aged TAMSD growth is observed also increases, see the estimation of equation (A22).

Ultimately, for even larger values of α for long ageing times t_a the transition from the linear to the ballistic behavior of $\left\langle\overline{\delta_a^2(\Delta)}\right\rangle$ is delayed so dramatically, that for the length of the trajectory examined in our computer simulations of figure AA4(b) the long-lag-time linear behavior is not present at all. These general features of the behavior of the aged TAMSD agree well with our theoretical predictions of equations (A19), (A20) and (A21), see figures AA3(b) and AA4(b). The magnitude of $\left\langle\overline{\delta_a^2(\Delta)}\right\rangle$ at intermediate lag times is well described by equation (A20) at $\alpha T\ll 1$ (see figure AA3(b)), while for larger α values (when this condition does not hold any longer) the magnitude of $\left\langle\overline{\delta_a^2(\Delta)}\right\rangle$ is, as expected, not well captured by the theory, with its linear slope is still correctly predicted (see figure AA4(b)).

3.1.2. Massless particles. The results of computer simulations in the overdamped limit of equation (14) demonstrate that the short-time evolution of $\left\langle x^2(t)\right\rangle$ for the massless particles is linear in time, see equation (A25). The MSD in the region of intermediate-to-long times grows exponentially with diffusion time, in agreement with the theoretical prediction of equations (A23) and (A24), as shown in figure 5. The variation of $\left\langle\overline{\delta^2(\Delta)}\right\rangle$ with the lag time obtained in simulations agrees with the analytical prediction (A26). In the limit of short lag times and long trajectories, the mean TAMSD grows linearly with Δ, in agreement with equation (A27). In this limit, the system behaves nonergodically: the magnitudes of $\left\langle x^2(\Delta)\right\rangle$ and $\left\langle\overline{\delta^2(\Delta)}\right\rangle$ differ by a large factor given by equation (A28). Toward the end of the trajectory, the MSD and mean TAMSD become equal, as predicted theoretically, see equation (A29). Note that the exponential growth of the MSD and the linear growth of the TAMSD are reminiscent of those known for geometric BM [202, 203], a paradigmatic stochastic process (effectively, exponentiated BM) modeling important features of price fluctuations (and respective returns) of the stock markets and option prices, see the fundamental studies [204, 205].

Therefore, the behavior of the MSD and mean TAMSD for ESBM for the massive and massless particles with $D(t)=D_0e^{2\alpha t}$ demonstrates that the long-time diffusion is dramatically different in the limit of underdamped and overdamped motion. Similar conclusions were made [121] for the case of canonical SBM [116] with a power-law variation of the diffusion coefficient with time, equation (2).

For the massless particles with $D(t)=D_0e^{2\alpha t}$ the ageing effects are much more pronounced than those for the massive particles, compare the results of computer simulations in figures 6 and AA3(b), respectively. Namely, for zero-mass particles the magnitudes of the aged MSD and aged TAMSD grow exponentially with the ageing time t_a. Specifically, the analytical expressions (A30) and (A31) quantify the Δ-independent universal rescaling for the ratio of the aged and nonaged spreading characteristics,

$$\frac{\left\langle x_a^2(\Delta)\right\rangle}{\left\langle x^2(\Delta)\right\rangle}=\frac{\left\langle\overline{\delta_a^2(\Delta)}\right\rangle}{\left\langle\overline{\delta^2(\Delta)}\right\rangle}=e^{2\alpha t_a}, \tag{26}$$

which are in excellent agreement with the results of simulations, see figure 6. The analytical expressions for the nonaged MSD and the mean TAMSD for zero-mass particles entering equation (26) are given by (A23) and (A26). Overall, for the massless particles the increase of $\left\langle\overline{\delta_a^2(\Delta)}\right\rangle$ with the ageing time t_a is considerably stronger than that of $\left\langle\overline{\delta_a^2(\Delta)}\right\rangle$ for the massive particles with $D(t)=D_0e^{2\alpha t}$.

As follows from figure 6 and equation (26) the phenomenon of weak ergodicity breaking (WEB) also prevails for aged

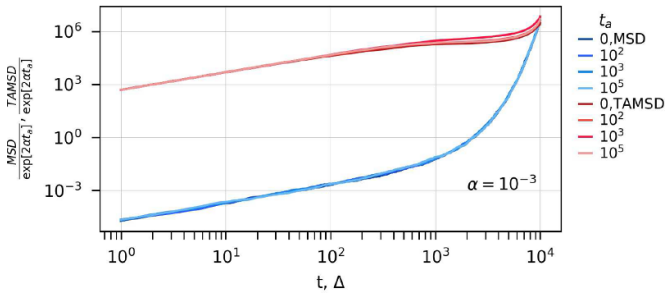

Figure 6. Aged MSD $\langle x_a^2(t)\rangle$ and aged mean TAMSD $\left\langle \overline{\delta_a^2(\Delta)}\right\rangle$ obtained by computer simulations of the *massless* particles with $D(t) = D_0 e^{2\alpha t}$ plotted versus the lag time Δ for varying ageing time t_a. The magnitudes of $\langle x_a^2(t)\rangle$ and $\left\langle \overline{\delta_a^2(\Delta)}\right\rangle$ were divided by the rescaling 'ageing' factor $e^{2\alpha t_a}$ (derived in equations (A30) and (A31), as shown on the y-axis) to yield the universal theoretically expected curve, equation (26). The values of t_a are given in the legend. Parameters: $m = 0$, $D_0 = 10^{-5}$, $\alpha = 10^{-3}$, $T = 10^4$, and $N = 10^3$.

ESBM describing the dynamics of the massless particles with $D(t) = D_0 e^{2\alpha t}$, with the MSD-to-TAMSD interrelation being similar to equation (A28) for the nonaged situation.

3.2. EB for $D(t) = D_0 e^{2\alpha t}$

3.2.1. Massive particles. The simulations for the massive particles with $D(t) = D_0 e^{2\alpha t}$ show that the EB parameter (9) at short lag times Δ does not grow linearly with Δ at a fixed trajectory length T, see figure AA5. EB attains rather large values at short lag times and the overall EB(Δ)-variation is quite weak. At a fixed lag time EB scales inversely proportional to the trace length,

$$\mathrm{EB}(T) \sim 1/T, \tag{27}$$

as demonstrated in figure AA6. This feature is similar to that for a number of other stochastic diffusion processes, both of normal and anomalous nature [10]. For comparison, in figure AA7 we present the EB variation versus the lag time for the case of time-independent diffusivity, at $\alpha = 0$.

For larger values of α the EB behavior with the lag time is more complicated, see figure AA8. Namely, after the initial decrease of EB with the trajectory length, roughly as $\mathrm{EB}(T) \propto 1/T$, at lag times $\Delta \gtrsim 1/\alpha$ the EB parameter starts (rather unexpectedly) *increasing* with T and it saturates at a plateau toward the very end of the trajectory, at $\Delta \to T$. The height of this plateau decreases as the lag time increases, see figure AA8.

3.2.2. Massless particles. For the massless particles with $D(t) = D_0 e^{2\alpha t}$ for the same α values we, however, still observe an $\mathrm{EB}(T) \sim 1/T$ decrease at a fixed lag time, see figure AA9. At $\Delta \gtrsim 1/\alpha$ the EB parameter stops decreasing, saturating at a pronounced plateau. The height of this EB plateau increases as the lag time increases, see figure AA9, a clear characteristic of a progressively less ergodic diffusion. We remind the reader that, as given by equation (9), when the dispersion of individual TAMSDs stays nearly unchanged for a constant lag time at varying trace lengths T, a plateau-like behavior of EB(T) is expected.

At $\Delta \gtrsim 1/\alpha$ the EB parameter starts experiencing the effects of ever growing diffusivity with time, $D(t) = D_0 e^{2\alpha t}$, and as a result at a fixed lag time Δ with an increasing length T of the trajectory the system does not reveal a progressively more ergodic behavior (with a decreasing EB value), but rather at $\alpha\Delta \gtrsim 1$ the EB parameter as a function of T attains a nearly constant, stationary value (see figure AA10 avialble online at (stacks.iop.org/JPD/54/195401/mmedia)). This behavior is consistent with a roughly linear EB(Δ) growth at short-to-intermediate lag times (in the region of lag times $\Delta \lesssim 1/\alpha$). Specifically, the functional variation of EB(Δ) is similar to that known for BM [10, 77],

$$\mathrm{EB}_{\mathrm{BM}}(\Delta) \approx 4\Delta/(3T), \tag{28}$$

but the observed magnitude of EB for ESBM with $D(t) = D_0 e^{2\alpha t}$ is considerably larger, see figure AA10. At later lag times, for Δ values in the range $1/\alpha \lesssim \Delta \lesssim T$, a nearly constant EB value is detected. Toward the very end of the trajectory, the magnitude of EB reveals a sharp growth to the terminal value of EB = 2, see figure AA10. This later part of the EB(Δ)-behavior for ESBM with $D(t) = D_0 e^{2\alpha t}$ is reminiscent of that for the EB parameter for the Ornstein–Uhlenbeck process (computed analytically and enumerated by simulations in [200] (for the equilibrium initial conditions of the harmonically confined particles), see also [201]).

We therefore observe that for the massive particles with $D(t) = D_0 e^{2\alpha t}$ the initial decrease of the EB parameter with T reverses into a transient increase at $T \gtrsim 1/\alpha$ (see figure AA8), while for the massless particles performing the same ESBM the EB parameter exhibits a plateau region in this range of trace-lengths. For short trajectories, when $T \lesssim 1/\alpha$ and the effects of a time-growing diffusivity are not yet manifesting themselves, the EB decreases with T similarly both for massive and massless particles.

4. Summary and discussion of the main results

In this study we presented the results of the analytical and computer-simulations-based analysis of anomalous and nonergodic diffusion (also in the presence of ageing) for the case of time-dependent diffusivity of the antagonistic forms $D(t) = D_0 e^{\pm 2\alpha t}$ (exponentially fast variation) and $D(t) = D_0 \log[t/\tau_0]$ (ultraslow logarithmic variation). Other than power-law, exponential, and logarithmic forms of the diffusivity variation in time can clearly be proposed for physical systems featuring other functional dependencies of $D(t)$. We summarize the key asymptotic results for the MSD and mean TAMSD for these three cases below as well as in table 1.

4.1. Case $D(t) = D_0 e^{2\alpha t}$

4.1.1. Massive particles. For the case of ESBM with $D(t) = D_0 e^{2\alpha t}$ the behavior of the nonaged system of the *massive*

particles is ergodic. Namely, we find the equivalence of the MSD $\langle x^2(t)\rangle$ and the mean TAMSD $\left\langle \overline{\delta^2(\Delta)}\right\rangle$ at short times (see equations (A6) and (A11)), as illustrated in figures 2, 3, and AA1. At log times $\left\langle \overline{\delta^2(\Delta)}\right\rangle$ can experience a drop in magnitude, as seen in figure AA2, while the MSD remains diffusive at long times, see figure 3.

For the aged system of the *massive* particles with $D(t) = D_0 e^{2\alpha t}$ the magnitude of the short-time ballistic MSD $\langle x_a^2(t)\rangle$ does not change with t_a, see equation (A18) and figures 4 and AA3(a). The magnitude of the aged mean TAMSD $\left\langle \overline{\delta_a^2(\Delta)}\right\rangle$ is ballistic at short times (at $\Delta \lesssim 1/\gamma_0$) and turns linear at intermediate-to-long times with the magnitude that increases with the ageing time t_a. This enhanced TAMSD magnitude is quantified by equation (A15) and it is shown in figure AA3(b). The results of computer simulations for $\left\langle \overline{\delta_a^2(\Delta)}\right\rangle$ of other values of α are also shown in figure AA4. We find that for very small α values, such that $\alpha T \ll 1$, the effect of ageing for $\alpha t_a \ll 1$ is negligible, see figure AA4(a). For longer ageing times t_a the region of the initial ballistic, ageing-independent growth $\left\langle \overline{\delta_a^2(\Delta)}\right\rangle \sim D_0\gamma_0\Delta^2$ extends in the region of longer lag times. Due to this, the respective $\left\langle \overline{\delta_a^2(\Delta)}\right\rangle$ increases with t_a as well, see figures AA3(b) and AA4(b) and equation (A20). For the aged system of *massive* particles with $D(t) = D_0 e^{2\alpha t}$ in the limit $\Delta/T \ll 1$ we observe no phenomenon of WEB, with the magnitudes of the aged MSD and aged mean TAMSD being equal at short (lag) times, see figures 4, AA3, and AA4.

4.1.2. Massless particles. For the nonaged system of the *massless* particles diffusing with $D(t) = D_0 e^{2\alpha t}$ the magnitudes of the MSD and mean TAMSD differ strongly in the limit of short (lag) times, compare equations (A25) and (A27). This fact is indicative of the presence of WEB, as demonstrated in figure 5 and table 1. We emphasize here the overall general trend of the MSD-to-TAMSD equivalence for the short-time underdamped diffusion versus the existence of WEB and the disparity in MSD-vs-TAMSD magnitudes for the short-time overdamped diffusion with $D(t) = D_0 e^{\pm 2\alpha t}$ and $D(t) = D_0 \log[t/\tau_0]$.

For short times the $\langle x^2(t)\rangle$ and $\left\langle \overline{\delta^2(\Delta)}\right\rangle$ grow linearly with time, while at intermediate-to-long times (at $t \gtrsim 1/\alpha$) the MSD scales exponentially, see equation (A24). This is in stark contrast to the at-most ballistic growth of the MSD predicted and observed for ESBM of the massive particles with $D(t) = D_0 e^{2\alpha t}$, as shown in figure 4.

Likewise, the magnitudes of the aged MSD $\langle x_a^2(t)\rangle$ and aged mean TAMSD $\left\langle \overline{\delta_a^2(\Delta)}\right\rangle$ for the situation $m = 0$ relate to their nonaged analogues in the very same proportions, see equations (A30) and (A31). The behavior of the overdamped ESBM system with $D(t) = D_0 e^{2\alpha t}$ is thus nonergodic in the presence of ageing as well. We emphasize that the magnitude of $\left\langle \overline{\delta_a^2(\Delta)}\right\rangle \Big/ \left\langle \overline{\delta^2(\Delta)}\right\rangle$ grows exponentially with the ageing time t_a, see equation (A31) and figure 6. For the nonaged and aged situations (for the long enough trajectories, at $\alpha T \gg 1$) at short (lag) times the magnitude of the mean TAMSD is much larger than that of the MSD. The respective proportionality factor is the exponential function of the trajectory length T, as given by the theoretical predictions (A28) and confirmed by the results of simulations presented in figures 5 and 6.

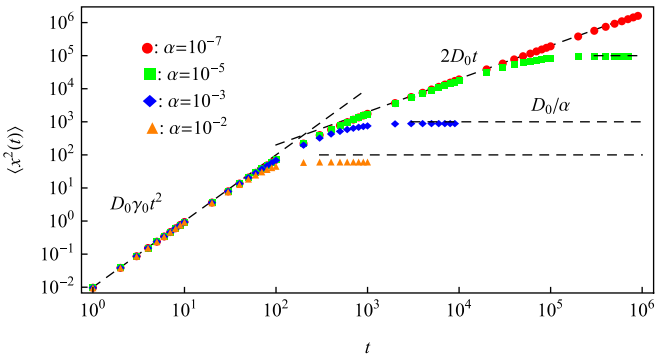

Figure 7. MSD for $D(t) = D_0 e^{-2\alpha t}$ for the *massive* particles (evaluated for the parameters as in simulations-based figure BB1 ($D_0 = 1$, $\gamma_0 = 10^{-2}$, and $T = 10^6$)) and plotted according to the full analytical expression (B2). The values of parameter α are provided in the legend. The short-time ballistic asymptote (B3), the intermediate-time linear diffusion law (B5), and the long-time stationary plateau of the MSD (B4) are the dashed horizontal lines (for the respective α values).

4.2. Case $D(t) = D_0 e^{-2\alpha t}$

4.2.1. Massive particles. The MSD for the *massive* particles with $D(t) = D_0 e^{-2\alpha t}$ is predicted theoretically by equation (B2) and presented in figure 7. Specifically, we find that after the initial ballistic regime (B3) at short times, the system features a linear growth of the MSD (B5) at intermediate times (in the regime $1/\gamma_0 \lesssim t \lesssim 1/\alpha$), and, ultimately, at long times the MSD saturates to a plateau (with the magnitude given by equation (B4)). These analytical predictions are in quantitative agreement with the findings from our stochastic computer simulations, as demonstrated in figure BB1 (for the same model parameters as in figure 7; see also figure BB2). According to the MSD and mean TAMSD expressions (B3) and (B8), respectively, and as demonstrated by the simulations in figure BB3, at short (lag) times the MSD and mean TAMSD are equal in magnitude and thus the ergodicity is preserved for ESBM with $D(t) = D_0 e^{-2\alpha t}$.

For the aged MSD $\langle x_a^2(t)\rangle$ of the *massive* particles with $D(t) = D_0 e^{-2\alpha t}$ the analytical expression (B11) is obtained. The transitions from the ballistic evolution of the MSD (B12) to the ageing-renormalized linear growth of $\langle x_a^2(t)\rangle$ (B13), and, later, from the linearly growing $\langle x_a^2(t)\rangle$ to the ageing-renormalized plateau given by equation (B14) are predicted. The aged MSD behaviors are illustrated in figure 8 (see also figure BB3 for the results of computer simulations). The behavior of the aged mean TAMSD $\left\langle \overline{\delta_a^2(\Delta)}\right\rangle$ at short and intermediate times is quantified by equations (B15) and (B16),

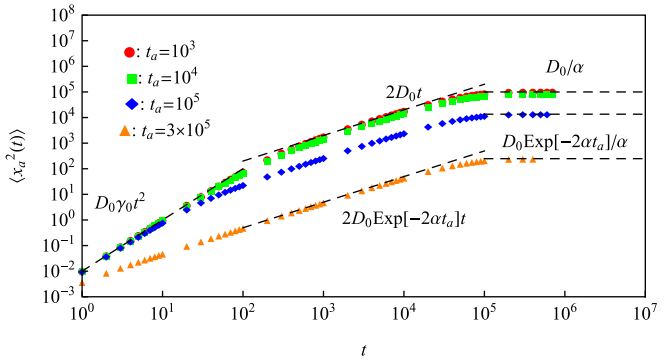

Figure 8. Aged MSD for $D(t)=D_0e^{-2\alpha t}$ for the *massive* particles as obtained from the general analytical expression (B11). The short-time ballistic asymptote (B12), the intermediate-time linear aged asymptote (B13), and the long-time ageing-renormalized plateau value (B14) are shown by the dashed lines. The values of the ageing time are given in the legend. Parameters: $m=1$, $T=10^7$, $D_0=1$, $\gamma_0=10^{-2}$, $\alpha=10^{-5}$.

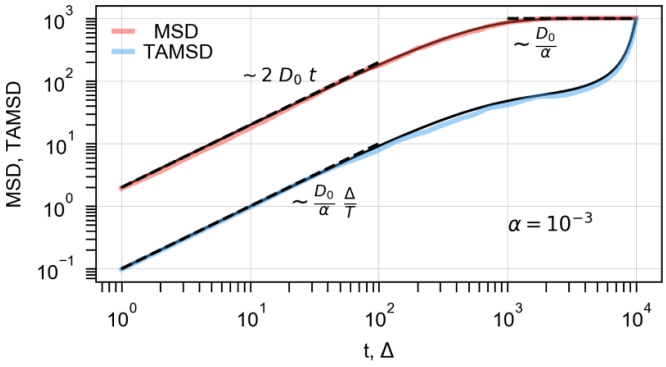

Figure 9. MSD $\langle x^2(t)\rangle$ and mean TAMSD $\left\langle\overline{\delta^2(\Delta)}\right\rangle$ for the *massless* particles with $D(t)=D_0e^{-2\alpha t}$. Full analytical predictions (B19) and (B20) are shown as the solid black curves. The short-time MSD asymptote (B21), short-lag-time TAMSD asymptote (B22), and the long-time MSD plateau (B23) are shown as the dashed lines. Parameters: $m=0$, $D_0=1$, $\alpha=10^{-3}$, $T=10^4$, and $N=10^3$.

withe the magnitude of the aged TAMSD decreasing with the ageing time. The overall behavior of the aged system of massive particles is ergodic at short times, see figure BB3 and also table 1.

4.2.2. Massless particles. For the *massless* particles performing ESBM with $D(t)=D_0e^{-2\alpha t}$ the MSD starts linearly at short times and reaches a plateau at long times, see equations (B21) and (B23), respectively. The magnitudes of the MSD $\langle x^2(t)\rangle$ and of the mean TAMSD $\left\langle\overline{\delta^2(\Delta)}\right\rangle$ in the limit of short (lag) times differ according to equations (B21) and (B22) and thus ergodicity in this system is weakly broken, as clearly visible from figure 9. For the overdamped limit of $D(t)=D_0e^{-2\alpha t}$ at short (lag) times the mean TAMSD is (much) smaller than the MSD (that is in contrast to the case with $D(t)=D_0e^{2\alpha t}$), see figure 9. The proportionality of $\langle x^2(t)\rangle$ and $\left\langle\overline{\delta^2(\Delta)}\right\rangle$ is quantified by equation (B22), with the prefactor scaling as a power-law-function of the trajectory length T. For ESBM with $D(t)=D_0e^{-2\alpha t}$ the intermediate-time MSD behavior and the long-time MSD plateau are found to be the same in the under- and overdamped limits, compared figures 7 and 9.

Likewise, in the presence of ageing, for the *massless* ESBM particles with $D(t)=D_0e^{-2\alpha t}$ the aged MSD $\langle x_a^2(t)\rangle$ and the aged mean TAMSD $\left\langle\overline{\delta_a^2(\Delta)}\right\rangle$ differ in the same proportions as in the nonaged situation, see equations (B25) and (B26), correspondingly. Therefore, at these conditions we observe WEB in the limit of short (lag) time as well, see figure BB4. For the ageing ESBM with $D(t)=D_0e^{-2\alpha t}$ the MSD magnitude is found to be reduced by the same exponential factor (B25) for the massive and massless particles, compared figures 8 and BB4. For the aged TAMSD the reduction of the ratio $\left\langle\overline{\delta_a^2(\Delta)}\right\rangle\Big/\left\langle\overline{\delta^2(\Delta)}\right\rangle$ is also exponential for the massless particles, see equation (B26). The collection of the main results is presented in table 1.

4.3. Case $D(t)=D_0\log[t/\tau_0]$

4.3.1. Massive particles. For the *massive* particles with $D(t)=D_0\log[t/\tau_0]$ we find that the MSD at short times grows ballistically, whereas at long times the logarithmic correction to the standard diffusion law is found, see equations (C8) and (C14) as well as the results of figures CC2 and 10. The mean TAMSD follows the ballistic asymptote (C18) in the limit of short and the logarithmically corrected linear-diffusion asymptote given by equation (C20) in the limit of long lag times.

For LSBM of the massive particles with $D(t)=D_0\log[t/\tau_0]$ the aged MSD starts with the same ballistic behavior at short times, equation (C23), and turns into the log-linear dependence (C26) at long times, with rather weak effects of the actual value of the ageing time t_a on the magnitude of $\langle x_a^2(t)\rangle$, see the theoretical results in figure 11 and the findings of computer simulations in figure CC3. The aged mean TAMSD at short (C29) and intermediate-to-long (C30) lag times is in the leading order equal in magnitude to the aged MSD, so that the ergodicity is maintained in the aged system of massive particles with $D(t)=D_0\log[t/\tau_0]$. Thus, similarly to the cases of $D(t)=D_0e^{\pm2\alpha t}$, in this case the behavior of both the nonaged and aged system is mostly ergodic at short times, contrary to that of the massless particles with a dramatic disparity in the magnitudes of the MSD and mean TAMSD, see also table 1.

4.3.2. Massless particles. For the *massless* particles with $D(t)=D_0\log[t/\tau_0]$ the nonaged MSD $\langle x^2(t)\rangle$ at short times is ballistic, see equation (C32) as well as figure CC4. In contrast, at short lag times the mean TAMSD $\left\langle\overline{\delta^2(\Delta)}\right\rangle$ exhibits a linear growth quantified by equation (C36), see figure CC4. The system thus exhibits WEB in this regime. The log-like 'weak' correction to the diffusion law for $D(t)=D_0\log[t/\tau_0]$ predicted analytically (C33) is verified by computer simulations in figure CC5 (see also figure 10). The logarithmic rescaling of the $\langle x_a^2(t)\rangle$ and $\left\langle\overline{\delta_a^2(\Delta)}\right\rangle$ predicted analytically by equations

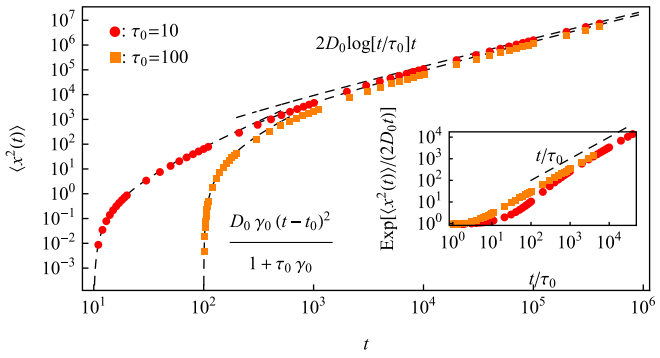

Figure 10. Analytical MSD for the case of *massive* particles with $D(t) = D_0 \log[t/\tau_0]$ obtained by numerical *integration* of equation (C6) (shown as the data points), with the asymptotic diffusion law at short times (C8) and the long-time log-linear prediction (C14) (both shown as the dashed black curves). The inset demonstrates the validity of the log-like correction to the standard diffusion law, as specified in equation (C34). Parameters: $D_0 = 1$, $\tau_0 = 10$ and 100 (see the legend), $\gamma_0 = 0.01$.

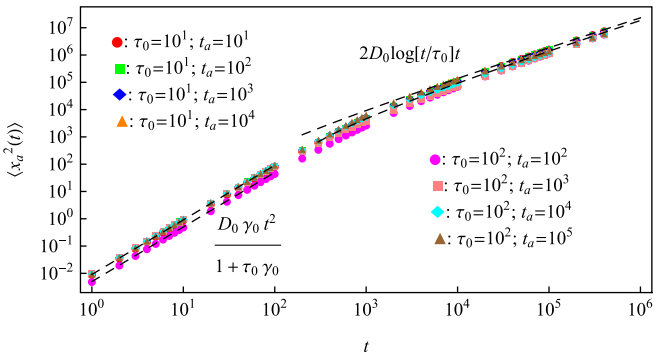

Figure 11. Aged MSD for the *massive* particles with $D(t) = D_0 \log[t/\tau_0]$ obtained via numerically integration of (C21) for varying values of the ageing time t_a as given in the legends (the data points). The short-time asymptote (C22) and the long-time law (C14) are the dashed curves. Parameters: $D_0 = 1$, $\tau_0 = 10$ and 100 (see the legends), and $\gamma_0 = 0.01$.

(C40) and (C41) is quantitatively confirmed by computer simulations, as shown in figure CC6.

Likewise, in the presence of ageing for the massless particles with $D(t) = D_0 \log[t/\tau_0]$ the magnitudes of the aged MSD $\langle x_a^2(t)\rangle$ given by equation (C38) and of the aged mean TAMSD $\left\langle \overline{\delta_a^2(\Delta)} \right\rangle$ in (C39) are not equal, and the system exhibits WEB, as quantified by (C42). For the massless particles with $D(t) = D_0 \log[t/\tau_0]$ the log-like enhancement of the magnitude of $\langle x_a^2(t)\rangle$ is observed, see equation (C40), while for the massive particles the log-linear diffusion law (C14) for $\langle x_a^2(t)\rangle$ remains almost unaffected by the duration of ageing, compare figures CC6(a) and 11.

5. Water time-dependent diffusion in the brain slows down with time

In this section, we discuss one biophysical application of the models with time-dependent diffusivity of power-law-like, exponential, and logarithmic functional forms, namely, the diffusion of water molecules in brain tissues.

5.1. Observations and definitions

Shortly, white matter of the brain mainly consists of myelinated axons (a high content of fatty lipids in the myelin sheath surrounding an axon), while gray matter is mainly composed of neurons. Water diffusion in white matter of a 'normal' human brain takes place considerably faster along the axonal tracts, while gray matter lacks such oriented fiber structures and features more isotropic diffusion [135]. Water diffusion in neural tissues—inherently restricted and anisotropic due to the presence of axonal bundles or neurofibrills—is affected by compartmentalization effects on the μm-scale (the diameter of a typical axon) [135].

Historically, the time-dependent diffusion $D(t)$ in different brain regions *in vivo* for a time range from 40 to 800 ms was observed [125] and qualitatively understood as diffusion in porous media and with semipermeable barriers or compartments [206]. The quality of diffusion-weighted magnetic-resonance imaging (dMRI) acquisition rapidly improves in recent years and enables the investigation of *in vivo* mesoscopic effects and quantification of axonal fibers connectivity and alignment [127].

One should distinguish the physical/apparent or cumulative [132] diffusion coefficient

$$D(t) = \mathrm{MSD}(t)/(2t) \tag{29}$$

and the coefficient of instantaneous diffusion,

$$D_{\mathrm{inst}}(t) = \frac{1}{2}\partial \mathrm{MSD}(t)/\partial t. \tag{30}$$

The latter relation actually leads to the $D(t)$ definition similar to that for the TAMSD (7), namely [127]

$$D(t) = \frac{1}{t}\int_0^t D_{\mathrm{inst}}(t')dt'. \tag{31}$$

The homogenization procedure used in the data analysis also yields nonzero, time-dependent higher-order cumulants (the so called diffusional kurtosis) [132]. The latter measures the residual inhomogeneity of the medium and indicates incomplete coarse-graining [132] of disordered microstructure as well as water exchange between neighboring compartments [132]. Performing coarse-graining in disordered systems at multiple scales—as typically required for biological tissues, at a progressively increasing diffusion length $l_d(t)$—yields the notion of time-dependent non-Gaussian diffusion [130]. The absence of a stationary diffusivity value is consistent with observation of anomalous diffusion at respective length- and time-scales, also indicating the absence of medium homogenization on this scale [130].

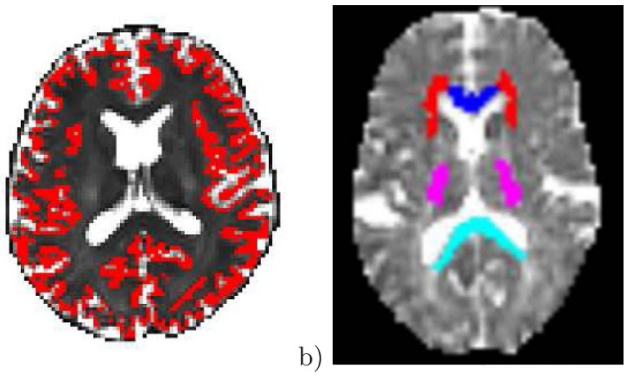

Figure 12. (a) dMRI scan showing regions of cortical gray matter featuring power-law-like variations of the diffusion coefficient, see equation (32). In red domains the cumulative $D(t)$ was averaged, with the power-law exponent $\vartheta \approx 1/2$ being measured for different individual gray-matter regions. The image is reproduced from [132], with permission of Elsevier. (b) The regions of white matter where cumulative $D(t)$ of the form (37) was observed [128] for diffusion-tensor eigenvalues transverse to the main white-matter tracts. The image is reproduced from [128], with permission of Elsevier.

5.2. Realizable D(t) forms and physical rationale

Mathematically, the two-compartment-based model was rationalized [207] to quantify water diffusion in the brain using some concepts of the Kärger exchange-diffusivity model [208]. On the time scales longer than the correlation time for a single compartment of the medium, the $D(t)$ follows an inverse power law of the universal form [126, 128, 131–133]

$$D(t) = D_\infty + A_\vartheta \times t^{-\vartheta}. \tag{32}$$

Here D_∞ is the long-time diffusivity and

$$\vartheta = (d+p)/2 < 1 \tag{33}$$

is the dynamical scaling exponent (which is half the sum of the spatial dimensionality of the compartments d and the structural exponent p). The latter describes inhomogeneities of a disordered microstructure of the medium [132] defining its universality class [130]. Experimentally, for dMRI of water diffusion in the brain [134], the compartmentalized microstructure of gray-matter tissues was shown to yield inverse-power-law cumulative $D(t)$ described by (32), see figure 12(a). As dMRI measures the cumulative $D(t)$, the power-law dependence observed in experiments is never faster than $D(t) \sim 1/t$ [209].

The theoretical basis for $D(t)$ of the form (32) with $\vartheta = 1/2$ was developed [210] for any space dimension d using the concepts of spatially restricted motion of the molecules by disorderly positioned and oriented semipermeable membrane-like barriers. The long-time diffusivity in (32) is assumed theoretically and measured experimentally to dominate the overall diffusivity magnitude yielding the long-time Gaussian diffusion, whereas small time-dependent corrections to it are treated as perturbations, resulting in non-Gaussian diffusion at that time scale. The time-dependent diffusivity itself is indicative of not yet-complete coarse-graining procedure.

For human cortical gray matter $D(t)$ was measured to reveal a weak and rather noisy dependence at up to 100 ms, with $\vartheta \approx 0.68$ (see, e.g. figure 3(b) in [132]). Note that experimental limitations on the dMRI-accessible time-range hamper the determination of the exact functional form of $D(t)$ decreasing with time as well as the actual exponent ϑ. Accessing short-time data could help the analysis to unambiguously clarify the precise functional dependence of $D(t)$ (power-law or exponential decay, or a superposition of these two $D(t)$ forms) [209].

For dMRI, the typical scale of medium heterogeneities is controlled by the diffusion length,

$$l_d(t) \sim \sqrt{\mathrm{MSD}(t)} \sim 1, \ldots, 50\ \mu\mathrm{m}, \tag{34}$$

corresponding to diffusion times $t_d \sim 1, \ldots, 10^3$ ms [130]. In neuronal tissues, the clinically employed dMRI diffusion times are $t_d \sim 10, \ldots, 10^2$ ms [127]. More heterogeneous samples lead to a slower approach to stationarity and, thus, smaller values of the dynamical exponent ϑ [130] for $D(t)$ in (32).

Totally regular environments give rise to a quick, exponential relaxation of the instantaneous diffusivity to its long-time value [127, 130],

$$D_{\mathrm{inst}}(t) = D_\infty + A_{\mathrm{exp}} \times \exp^{-t/t_c}, \tag{35}$$

and the value of the p exponent in (33) goes to infinity [130]. Exponential decay can occur for $D_{\mathrm{inst}}(t)$, but for the cumulative $D(t)$ was not yet observed experimentally in the brain [209]. Note, however, that to quantitatively distinguish between the two decreasing $D(t)$ forms (32) and (35) the dMRI measurements in a broader time-range are necessary [130]. In contrast, in the presence of strong fluctuations/irregularities the exponent p decreases, yielding a slower approach of $D(t)$ to stationarity (due to overall smaller ϑ). For $\vartheta > 1$ one gets [126–128]

$$D(t) = D_\infty + A_1 \times t^{-1} \tag{36}$$

and in this case water molecules are fully confined.

Finally, the diffusivity in the 'borderline case' $\vartheta = 1$ acquires mathematically a logarithmic dependence on time, in addition to a power law, namely [126–129, 132]

$$D(t) = D_\infty + A_{\log} \times \log[t/t_c]/t. \tag{37}$$

The diffusivity slowly approaching the macroscopic limit following (37) was proposed [127–129] to arise experimentally in water diffusion in white matter *in vivo*. A cumulative $D(t)$ of this form was observed for diffusion tensor eigenvalues transverse to main white-matter tracts [128]. It was proposed [128] that systematic $\sim \log t$-like deviations in $D(t)$ from the $\sim 1/t$ scaling occur as a consequence of short-range disorder in the extra-axonal space.

From the mathematical perspective, depending on one- or two-dimensional disorder, effectively, one gets different dynamical exponents in $D_{\mathrm{inst}}(t)$: namely, it is a $\sim t^{-1/2}$ scaling for one dimension (along white-mater fibers or along randomly oriented dendrites and axons in gray matter) and a

$\sim t^{-1}$ scaling for two dimensions (transverse to white-matter tracts) [209]. These dependencies in the $D_{\rm inst}(t)$ translate to $\sim t^{-1/2}$ and $\sim(\log t)/t$ functional forms in the cumulative $D(t)$, as follows from the definition, see equation (31) (we thank D Novikov for clarification [209]). Ball-like structural swellings irregularly occurring along axons modify the standard diffusion law [132] along them, from that in one dimension to that in the presence of interruptions and quasi-two-dimensional swollen regions. We emphasize also a large innate polydispersity existing for axon calibers [211].

5.3. Quantitative diagnostics based on D(t)-properties

From the diagnostic perspective, the dMRI is a sensitive technique for the detailed *in vivo* measurement of microstructural features of various biological tissues (both healthy and pathological) on the μm-scale [133]. Recent evidence of diffusion along major human-white-matter axonal tracts revealed non-Gaussian and nontrivially time-dependent diffusion [133]. In gray-matter tissues, $D(t)$-diffusion was also observed, making some diffusion features along axons and dendrites universal for neuronal tissues. The functional $D(t)$ form (32) was recently shown to be most sensitive to variations of the axon diameter/caliber along the fiber on the microscale (constructing thereby a heterogeneous landscape along a given tract) [133].

This fact offered the physical-biological rationale for restrictions of and impediments for water diffusion [133] shown mathematically [207] to yield $D(t)$ of the form (32). The parameters in (32) were demonstrated to be altered in patients with neurodegenerative diseases, such as multiple sclerosis [133]. Specifically, the value of the bulk diffusivity D_∞ was shown to increase in such pathological tissues, while the factor $A_{\rm exp}$ was revealed to decrease measurably and systematically, as compared to that in the healthy tissue [133]. These two model parameters are, thus, rather sensitive indicators for detecting certain pathological tissue regions and (hopefully) proposing a pertinent physical mechanism for such abnormalities in tissue functioning in terms of permeability by water, also shedding new light onto possible pathological mechanisms of formation of multiple-sclerosis lesion [133].

Acknowledgment

A G C thanks D S Novikov for enlightening discussions and correspondence. A G C is grateful to the Institute of Physics of HU Berlin and to Prof. I. M. Sokolov personally for support and hospitality. H S acknowledges the resources of the Center of High-Performance Computing, School of Biological Sciences (IPM). R M acknowledges financial support by the Deutsche Forschungsgemeinschaft (DFG Grant ME 1535/7-1). R M also thanks the Foundation for Polish Science (Fundacja na rzecz Nauki Polskiej) within an Alexander von Humboldt Polish Honorary Research Scholarship.

Conflicts of interest

There are no conflicts to declare.

Abbreviations

MSD, mean-squared displacement; TAMSD, time-averaged MSD; WEB, weak ergodicity breaking; BM, Brownian motion; SBM, scaled BM; ESBM, exponential SBM; LSBM, logarithmic SBM; dMRI, diffusion-weighted magnetic-resonance imaging.

ORCID iDs

Andrey G Cherstvy https://orcid.org/0000-0002-0516-9900
Ralf Metzler https://orcid.org/0000-0002-6013-7020

References

[1] Haus J W and Kehr K W 1987 Diffusion in regular and disordered lattices *Phys. Rep.* **150** 263
[2] Bouchaud J-P and Georges A 1990 Anomalous diffusion in disordered media: statistical mechanisms, models and physical applications *Phys. Rep.* **195** 127
[3] Havlin S and Ben-Avraham D 2002 Diffusion in disordered media *Adv. Phys.* **51** 187
[4] Metzler R and Klafter J 2000 The random walk's guide to anomalous diffusion: a fractional dynamics approach *Phys. Rep.* **339** 1
[5] Burov S, Jeon J-H, Metzler R and Barkai E 2011 Single particle tracking in systems showing anomalous diffusion: the role of weak ergodicity breaking *Phys. Chem. Chem. Phys.* **13** 1800
[6] Barkai E, Garini Y and Metzler R 2012 Strange kinetics of single molecules in living cells *Phys. Today* **65** 29
[7] Sokolov I M 2012 Models of anomalous diffusion in crowded environments *Soft Matter* **8** 9043
[8] Saxton M J 2012 Wanted: a positive control for anomalous subdiffusion *Biophys. J.* **103** 2411
[9] Höfling F and Franosch T 2013 Anomalous transport in the crowded world of biological cells *Rep. Prog. Phys.* **76** 046602
[10] Metzler R, Jeon J-H, Cherstvy A G and Barkai E 2014 Anomalous diffusion models and their properties: non-stationarity, non-ergodicity and ageing at the centenary of single particle tracking *Phys. Chem. Chem. Phys.* **16** 24128
[11] Meroz Y and Sokolov I M 2015 A toolbox for determining subdiffusive mechanisms *Phys. Rep.* **573** 1
[12] Metzler R, Jeon J-H and Cherstvy A G 2016 Non-Brownian diffusion in lipid membranes: experiments and simulations *Biochem. Biophys. Acta* **1858** 2451
[13] Basak S, Sengupta S and Chattopadhyay K 2019 Understanding biochemical processes in the presence of sub-diffusive behavior of biomolecules in solution and living cells *Biophys. Rev.* **11** 851
[14] Banks D and Fradin C 2005 Anomalous diffusion of proteins due to molecular crowding *Biophys. J.* **89** 2960
[15] Golding I and Cox E C 2006 Physical nature of bacterial cytoplasm *Phys. Rev. Lett.* **96** 098102
[16] Szymanski J and Weiss M 2009 Elucidating the origin of anomalous diffusion in crowded fluids *Phys. Rev. Lett.* **103** 038102
[17] Bronstein I, Israel Y, Kepten E, Mai S, Shav-Tal Y, Barkai E and Garini Y 2009 Transient anomalous diffusion of telomeres in the nucleus of mammalian cells *Phys. Rev. Lett.* **103** 018102

[18] Wang B, Anthony S M, Bae S C and Granick S 2009 Anomalous yet Brownian *Proc. Natl Acad. Sci. USA* **106** 15160

[19] Weber S C, Spakowitz A J and Theriot J A 2010 Bacterial chromosomal loci move subdiffusively through a viscoelastic cytoplasm *Phys. Rev. Lett.* **104** 238102

[20] Jeon J-H, Tejedor V, Burov S, Barkai E, Selhuber-Unkel C, Berg-Sorensen K, Oddershede L and Metzler R 2011 In vivo anomalous diffusion and weak ergodicity breaking of lipid granules *Phys. Rev. Lett.* **106** 048103

[21] English B P, Hauryliuk V, Sanamrad A, Tankov S, Dekker N H and Elf J 2011 Single-molecule investigations of the stringent response machinery in living bacterial cells *Proc. Natl Acad. Sci. USA* **108** E365

[22] Ehrig J, Petrov E P and Schwille P 2011 Near-critical fluctuations and cytoskeleton-assisted phase separation lead to subdiffusion in cell membranes *Biophys. J.* **100** 80

[23] Kneller G R, Baczynski K and Pasenkiewicz-Gierula M 2011 Communication: consistent picture of lateral subdiffusion in lipid bilayers: molecular dynamics simulation and exact results *J. Chem. Phys.* **135** 141105

[24] Weigel A V, Simon B, Tamkun M M and Krapf D 2011 Ergodic and nonergodic processes coexist in the plasma membrane as observed by single-molecule tracking *Proc. Natl Acad. Sci. USA* **108** 6438

[25] Hellmann M, Heermann D W and Weiss M 2011 Anomalous reaction kinetics and domain formation on crowded membranes *Europhys. Lett.* **94** 18002

[26] Akimoto T, Yamamoto E, Yasuoka K, Hirano Y and Yasui M 2011 Non-Gaussian fluctuations resulting from power-law trapping in a lipid bilayer *Phys. Rev. Lett.* **107** 178103

[27] Jeon J-H, Monne H M, Javanainen M and Metzler R 2012 Anomalous diffusion of phospholipids and cholesterols in a lipid bilayer and its origins *Phys. Rev. Lett.* **109** 188103

[28] Goose J E and Sansom M S P 2013 Reduced lateral mobility of lipids and proteins in crowded membranes *PLoS Comput. Biol.* **9** e1003033

[29] Duncan A L *et al* 2017 Protein crowding and lipid complexity influence the nanoscale dynamic organization of ion channels in cell membranes *Sci. Rep.* **7** 16647

[30] Javanainen M, Hammaren H, Monticelli L, Jeon J-H, Miettinen M S, Martinez-Seara H, Metzler R and Vattulainen I 2013 Anomalous and normal diffusion of proteins and lipids in crowded lipid membranes *Faraday Discuss.* **161** 397

[31] Tabei S M A, Burov S, Kim H Y, Kuznetsov A, Huynh T, Jureller J, Philipson L H, Dinner A R and Scherer N F 2013 Intracellular transport of insulin granules is a subordinate *Proc. Natl Acad. Sci. USA* **110** 4911

[32] Yamamoto E, Akimoto T, Yasui M and Yasuoka K 2014 Origin of subdiffusion of water molecules on cell membrane surfaces *Sci. Rep.* **4** 4720

[33] Stachura S and Kneller G R 2014 Anomalous lateral diffusion in lipid bilayers observed by molecular dynamics simulations with atomistic and coarse-grained force fields *Mol. Simul.* **40** 245

[34] Skaug M J, Mabry J N and Schwartz D K 2014 Single-molecule tracking of polymer surface diffusion *J. Am. Chem. Soc.* **136** 1327

[35] Skaug M J and Schwartz D K 2015 Tracking nanoparticle diffusion in porous filtration media *Ind. Eng. Chem. Res.* **54** 4414

[36] Wang D, Hu R, Skaug M J and Schwartz D K 2015 Temporally anti-correlated motion of nanoparticles at a liquid interface *J. Phys. Chem. Lett.* **6** 54

[37] Krapf D 2015 Mechanisms underlying anomalous diffusion in the plasma membrane *Curr. Top. Membr.* **75** 167

[38] Manzo C, Torreno-Pina J A, Massignan P, Lapeyre Jr G J, Lewenstein M and Garcia-Parajo M F 2015 *Phys. Rev.* X **5** 011021

[39] Massignan P, Manzo C, Torreno-Pina J A, Garcia-Parajo M F, Lewenstein M and Lapeyre Jr G J 2014 Nonergodic subdiffusion from Brownian motion in an inhomogeneous medium *Phys. Rev. Lett.* **112** 150603

[40] Reverey J F, Jeon J-H, Bao H, Leippe M, Metzler R and Selhuber-Unkel C 2015 Superdiffusion dominates intracellular particle motion in the supercrowded cytoplasm of pathogenic *Acanthamoeba castellanii Sci. Rep.* **5** 11690

[41] Yamamoto E, Kalli A C, Akimoto T, Yasuoka K and Sansom M S P 2015 Anomalous dynamics of a lipid recognition protein on a membrane surface *Sci. Rep.* **5** 18245

[42] Jeon J-H, Javanainen M, Martinez-Seara H, Metzler R and Vattulainen I 2016 Protein crowding in lipid bilayers gives rise to non-Gaussian anomalous lateral diffusion of phospholipids and proteins *Phys. Rev.* X **6** 021006

[43] Babayekhorasani F, Dunstan D E, Krishnamoorti R and Conrad J C 2016 Nanoparticle diffusion in crowded and confined media *Soft Matter* **12** 8407

[44] Wagner T, Kroll A, Haramagatti C R, Lipinski H-G and Wiemann M 2017 Classification and segmentation of nanoparticle diffusion trajectories in cellular micro environments *PLoS One* **12** e0170165

[45] Golan Y and Sherman E 2017 Resolving mixed mechanisms of protein subdiffusion at the T cell plasma membrane *Nat. Commun.* **8** 15851

[46] Yamamoto E, Akimoto T, Kalli A C, Yasuoka K and Sansom M S P 2017 Dynamic interactions between a membrane binding protein and lipids induce fluctuating diffusivity *Sci. Adv.* **3** e1601871

[47] Lampo T J, Stylianidou S, Backlund M P, Wiggins P A and Spakowitz A J 2017 Cytoplasmic RNA-protein particles exhibit non-Gaussian subdiffusive behavior *Biophys. J.* **112** 532

[48] Stadler L and Weiss M 2017 Non-equilibrium forces drive the anomalous diffusion of telomeres in the nucleus of mammalian cells *New. J. Phys.* **19** 113048

[49] Song M S, Moon H C, Jeon J-H and Park H Y 2018 Neuronal messenger ribonucleoprotein transport follows an aging Lévy walk *Nat. Commun.* **9** 344

[50] Cherstvy A G, Nagel O, Beta C and Metzler R 2018 Non-Gaussianity, population heterogeneity and transient superdiffusion in the spreading dynamics of amoeboid cells *Phys. Chem. Chem. Phys.* **20** 23034

[51] Cherstvy A G, Thapa S, Wagner C E and Metzler R 2019 Non-Gaussian, non-ergodic and non-Fickian diffusion of tracers in mucin hydrogels *Soft Matter* **15** 2481

[52] Thapa S, Cherstvy A G, Lukat N, Selhuber-Unkel C and Metzler R 2019 Transient superdiffusion of polydisperse vacuoles in supercrowded amoeboid cells *J. Chem. Phys.* **150** 144901

[53] Anderson S J, Matsuda C, Garamella J, Peddireddy K R, Robertson-Anderson R M and McGorty R 2019 Filament rigidity vies with mesh size in determining anomalous diffusion in cytoskeleton *Biomacromolecules* **20** 4380

[54] Nousi A, Sogaard M T, and Jauffred L 2020 Single-cell tracking reveals super-spreading cells with high persistence in invasive brain cancer *bioRxiv preprint* (https://doi.org/10.1101/2020.10.06.327676)

[55] Coker H L E, Cheetham M R, Kattnig D R, Wang Y J, Garcia-Manyes S and Wallace M I 2019 Controlling anomalous diffusion in lipid membranes *Biophys. J.* **116** 1085

[56] Ye Z, Wang X and Xiao L 2019 Single-particle tracking with scattering-based optical microscopy *Anal. Chem.* **91** 15327

[57] Enkavi G, Javanainen M, Kulig W, Rog T and Vattulainen I 2019 Multiscale simulations of biological membranes: the challenge to understand biological phenomena in a living substance *Chem. Rev.* **119** 5607

[58] Xu Z, Gao L, Chen P and Yan L-T 2020 Diffusive transport of nanoscale objects with cell membranes: a computational perspective *Soft Matter* **16** 3869

[59] Astafiev A A, Shakhov A M, Osychenko A A, Syrchina M S, Karmenyan A V, Tochilo U A and Nadtochenko V A 2020 Probing intracellular dynamics using fluorescent carbon dots produced by femtosecond laser *in situ ACS Omega* **5** 12527

[60] Sabri A, Xu X, Krapf D and Weiss M 2020 Elucidating the origin of heterogeneous anomalous diffusion in the cytoplasm of mammalian cells *Phys. Rev. Lett.* **125** 058101

[61] Bohrer C H and Xiao J 2020 Complex diffusion in bacteria *Advances in Experimental Medicine and Biology* vol 1267 eds. G Dumenil and S van Teeffelen (Berlin: Springer) p 15

[62] He Y, Burov S, Metzler R and Barkai E 2008 Random time-scale invariant diffusion and transport coefficients *Phys. Rev. Lett.* **101** 058101

[63] Chechkin A V, Hofmann M and Sokolov I M 2009 Continuous-time random walk with correlated waiting times *Phys. Rev.* E **80** 031112

[64] Neusius T, Sokolov I M and Smith J C 2009 Subdiffusion in time-averaged, confined random walks *Phys. Rev.* E **80** 011109

[65] Magdziarz M, Metzler R, Szczotka W and Zebrowski P 2012 Correlated continuous-time random walks in external force fields *Phys. Rev.* E **85** 051103

[66] Schulz J H P, Barkai E and Metzler R 2013 Aging effects and population splitting in single-particle trajectory averages *Phys. Rev. Lett.* **110** 020602

[67] Schulz J H P, Barkai E and Metzler R 2014 Aging renewal theory and application to random walks *Phys. Rev.* X **4** 011028

[68] Akimoto T and Barkai E 2013 Aging generates regular motions in weakly chaotic systems *Phys. Rev.* E **87** 032915

[69] Akimoto T and Miyaguchi T 2010 Role of infinite invariant measure in deterministic subdiffusion *Phys. Rev.* E **82** 030102

[70] Hou R, Cherstvy A G, Metzler R and Akimoto T 2018 Biased continuous-time random walks for ordinary and equilibrium cases: facilitation of diffusion, ergodicity breaking and ageing *Phys. Chem. Chem. Phys.* **20** 20827

[71] Munoz-Gil G, Charalambous C, Garcia-March M A, Garcia-Parajo M F, Manzo C, Lewenstein M and Celi A 2017 Transient subdiffusion from an Ising environment *Phys. Rev.* E **96** 052140

[72] Charalambous C, Munoz-Gil G, Celi A, Garcia-Parajo M F, Lewenstein M, Manzo C and García-March M A 2017 Nonergodic subdiffusion from transient interactions with heterogeneous partners *Phys. Rev.* E **95** 032403

[73] Munoz-Gil G, Garcia-March M A, Manzo C, Celi A and Lewenstein M 2019 Diffusion through a network of compartments separated by partially-transmitting boundaries *Front. Phys.* **7** 31

[74] Goychuk I 2009 Viscoelastic subdiffusion: from anomalous to normal *Phys. Rev.* E **80** 046125

[75] Goychuk I 2012 Viscoelastic subdiffusion: generalized Langevin equation approach *Adv. Chem. Phys.* **150** 187

[76] Goychuk I 2018 Viscoelastic subdiffusion in a random Gaussian environment *Phys. Chem. Chem. Phys.* **20** 24140

[77] Deng W and Barkai E 2009 Ergodic properties of fractional Brownian-Langevin motion *Phys. Rev.* E **79** 011112

[78] Jeon J-H and Metzler R 2010 Fractional Brownian motion and motion governed by the fractional Langevin equation in confined geometries *Phys. Rev.* E **81** 021103

[79] Jeon J-H and Metzler R 2012 Inequivalence of time and ensemble averages in ergodic systems: exponential versus power-law relaxation in confinement *Phys. Rev.* E **85** 021147

[80] Burnecki K, Kepten E, Janczura J, Bronshtein I, Garini Y and Weron A 2012 Universal algorithm for identification of fractional Brownian motion. A case of telomere subdiffusion *Biophys. J.* **103** 1839

[81] Sarfati R and Schwartz D K 2020 Temporally anticorrelated subdiffusion in water nanofilms on silica suggests near-surface viscoelasticity *ACS Nano* **14** 304

[82] Fernandez A D, Charchar P, Cherstvy A G, Metzler R and Finnis M W 2020 The diffusion of doxorubicin drug molecules in silica nanoslits is non-Gaussian, intermittent and anticorrelated *Phys. Chem. Chem. Phys.* **22** 27955

[83] Jamali V, Hargus C, Ben-Moshe A, Aghazadeh A, Ha H D, Mandadapu K K and Alivisatos A P 2020 Anomalous nanoparticle surface diffusion in liquid cell TEM is revealed by deep learning-assisted analysis *preprint* (https://doi.org/10.26434/chemrxiv.12894050.v2)

[84] Lutz E 2001 Fractional Langevin equation *Phys. Rev.* E **64** 051106

[85] Lau A W C and Lubensky T C 2007 State-dependent diffusion: thermodynamic consistency and its path integral formulation *Phys. Rev.* E **76** 011123

[86] Polettini M 2013 Generally covariant state-dependent diffusion *J. Stat. Mech.* P07005

[87] Fulinski A 2013 Communication: how to generate and measure anomalous diffusion in simple systems *J. Chem. Phys.* **138** 021101

[88] Cherstvy A G, Chechkin A V and Metzler R 2013 Anomalous diffusion and ergodicity breaking in heterogeneous diffusion processes *New J. Phys.* **15** 083039

[89] Cherstvy A G and Metzler R 2013 Population splitting, trapping and non-ergodicity in heterogeneous diffusion processes *Phys. Chem. Chem. Phys.* **15** 20220

[90] Cherstvy A G, Chechkin A V and Metzler R 2014 Particle invasion, survival and non-ergodicity in 2D diffusion processes with space-dependent diffusivity *Soft Matter* **10** 1591

[91] Cherstvy A G, Chechkin A V and Metzler R 2014 Ageing and confinement in non-ergodic heterogeneous diffusion processes *J. Phys.* A **47** 485002

[92] Cherstvy A G and Metzler R 2014 Nonergodicity, fluctuations and criticality in heterogeneous diffusion processes *Phys. Rev.* E **90** 012134

[93] Cherstvy A G and Metzler R 2015 Ergodicity breaking, ageing and confinement in generalized diffusion processes with position and time dependent diffusivity *J. Stat. Mech.* **P05010**

[94] Kazakevicius R and Ruseckas J 2016 Influence of external potentials on heterogeneous diffusion processes *Phys. Rev.* E **94** 032109

[95] Leibovich N and Barkai E 2019 Infinite ergodic theory for heterogeneous diffusion processes *Phys. Rev.* E **99** 042138

[96] Wang W, Cherstvy A G, Liu X and Metzler R 2020 Anomalous diffusion and nonergodicity for heterogeneous diffusion processes with fractional Gaussian noise *Phys. Rev.* E **102** 012146

[97] Volpe G and Wehr J 2016 Effective drifts in dynamical systems with multiplicative noise: a review of recent progress *Rep. Prog. Phys.* **79** 053901

[98] Xu Y, Liu X, Li Y and Metzler R 2020 Heterogeneous diffusion processes and nonergodicity with Gaussian colored noise in layered diffusivity landscapes *Phys. Rev.* E **102** 062106

[99] Li Y, Guo W, Du L-C and Mei D-C 2019 Subdiffusion and ergodicity breaking in heterogeneous environments subject to Lévy noise *Physica* A **514** 948
[100] Angelani L and Garra R 2019 Run-and-tumble motion in one dimension with space-dependent speed *Phys. Rev.* E **100** 052147
[101] Wang X, Deng W and Chen Y 2019 Ergodic properties of heterogeneous diffusion processes in a potential well *J. Chem. Phys.* **150** 164121
[102] Sandev T, Schulz A, Kantz H and Iomin A 2018 Heterogeneous diffusion in comb and fractal grid structures *Chaos Solitons Fractals* **114** 551
[103] Sancho J M 2015 Brownian colloids in underdamped and overdamped regimes with nonhomogeneous temperature *Phys. Rev.* E **92** 062110
[104] Berry H and Chate H 2014 Anomalous diffusion due to hindering by mobile obstacles undergoing Brownian motion or Ornstein-Uhlenbeck processes *Phys. Rev.* E **89** 022708
[105] Trovato F and Tozzini V 2014 Diffusion within the cytoplasm: a mesoscale model of interacting macromolecules *Biophys. J.* **107** 2579
[106] Weiss M 2014 Crowding, diffusion and biochemical reactions *Int. Rev. Cell Mol. Biol.* **307** 383
[107] Saxton M J 2014 Wanted: scalable tracers for diffusion measurements *J. Phys. Chem.* B **118** 12805
[108] Jain R and Sebastian K L 2016 Diffusion in a crowded, rearranging environment *J. Phys. Chem.* B **120** 3988
[109] Ghosh S K, Cherstvy A G and Metzler R 2015 Non-universal tracer diffusion in crowded media of non-inert obstacles *Phys. Chem. Chem. Phys.* **17** 1847
[110] Ghosh S K, Cherstvy A G, Grebenkov D S and Metzler R 2016 Anomalous, non-Gaussian tracer diffusion in crowded two-dimensional environments *New J. Phys.* **18** 013027
[111] Russian A, Dentz M and Gouze P 2017 Self-averaging and weak ergodicity breaking of diffusion in heterogeneous media *Phys. Rev.* E **96** 022156
[112] dos Santos M A F and Junior L M 2020 Log-normal superstatistics for Brownian particles in a heterogeneous environment *MDPI Phys.* **2** 571
[113] Benichou O, Illien P, Oshanin G, Sarracino A and Voituriez R 2018 Tracer diffusion in crowded narrow channels *J. Phys.: Condens. Matter* **30** 443001
[114] Lim S C and Muniandy S V 2002 Self-similar Gaussian processes for modeling anomalous diffusion *Phys. Rev.* E **66** 021114
[115] Hottovy S, Volpe G and Wehr J 2012 Thermophoresis of Brownian particles driven by coloured noise *Europhys. Lett.* **99** 60002
[116] Jeon J-H, Chechkin A V and Metzler R 2014 Scaled Brownian motion: a paradoxical process with a time dependent diffusivity for the description of anomalous diffusion *Phys. Chem. Chem. Phys.* **16** 15811
[117] Thiel F and Sokolov I M 2014 Scaled Brownian motion as a mean-field model for continuous-time random walks *Phys. Rev.* E **89** 012115
[118] Safdari H, Cherstvy A G, Chechkin A V, Thiel F, Sokolov I M and Metzler R 2015 Quantifying the non-ergodicity of scaled Brownian motion *J. Phys.* A **48** 375002
[119] Bodrova A, Chechkin A V, Cherstvy A G and Metzler R 2015 Quantifying non-ergodic dynamics of force-free granular gases *Phys. Chem. Chem. Phys.* **17** 21791
[120] Bodrova A, Chechkin A V, Cherstvy A G and Metzler R 2015 Ultraslow scaled Brownian motion *New J. Phys.* **17** 063038
[121] Bodrova A, Chechkin A V, Cherstvy A G, Safdari H, Sokolov I M and Metzler R 2016 Underdamped scaled Brownian motion: (non-)existence of the overdamped limit in anomalous diffusion *Sci. Rep.* **6** 30520
[122] Safdari H, Cherstvy A G, Chechkin A V, Bodrova A and Metzler R 2017 Aging underdamped scaled Brownian motion: ensemble- and time-averaged particle displacements, nonergodicity and the failure of the overdamping approximation *Phys. Rev.* E **95** 012120
[123] Bodrova A S, Chechkin A V and Sokolov I M 2019 Scaled Brownian motion with renewal resetting *Phys. Rev.* E **100** 012120
[124] Guerrero B V, Chakraborty B, Zuriguel I and Garcimartin A 2019 Nonergodicity in silo unclogging: broken and unbroken arches *Phys. Rev.* E **100** 032901
[125] Horsfield M, Barker G and McDonald W 1994 Self-diffusion in CNS tissue by volume-selective proton NMR *Magn. Reson. Med.* **31** 637
[126] Novikov D S, Jensen J H, Helpern J A and Fieremans E 2014 Revealing mesoscopic structural universality with diffusion *Proc. Natl Acad. Sci. USA* **111** 5088
[127] Burcaw L M, Fieremans E and Novikov D S 2015 Mesoscopic structure of neuronal tracts from time-dependent diffusion *Neuroimage* **114** 18
[128] Fieremans E, Burcaw L M, Lee H H, Lemberskiy G, Veraart J and Novikov D S 2016 *In vivo* observation and biophysical interpretation of time-dependent diffusion in human white matter *Neuroimage* **129** 414
[129] Lee H-H, Fieremans E and Novikov D S 2018 What dominates the time dependence of diffusion transverse to axons: intra- or extra-axonal water? *Neuroimage* **182** 500
[130] Novikov D S, Fieremans E, Jespersen S N and Kiselev V G 2019 Quantifying brain microstructure with diffusion MRI: theory and parameter estimation *NMR Biomed.* **32** e3998
[131] Lee H-H, Papaioannou A, Kim S-L, Novikov D S and Fieremans E 2020 Probing axonal swelling with time dependent diffusion MRI *Commun. Biol.* **3** 354
[132] Lee H-H, Papaioannou A, Novikov D S and Fieremans E 2020 *In vivo* observation and biophysical interpretation of time-dependent diffusion in human cortical gray matter *Neuroimage* **222** 117054
[133] Lee H-H, Papaioannou A, Kim S-L, Novikov D S and Fieremans E 2020 A time-dependent diffusion MRI signature of axon caliber variations and beading *Commun. Biol.* **3** 354
[134] Barrick T R *et al* 2020 Quasi-diffusion magnetic resonance imaging (QDI): a fast, high b-value diffusion imaging technique *Neuroimage* **211** 116606
[135] Beaulieu C 2002 The basis of anisotropic water diffusion in the nervous system — a technical review *NMR Biomed.* **15** 435
[136] Capuani S and Palombo M 2020 Mini review on anomalous diffusion by MRI: potential advantages, pitfalls, limitations, nomenclature and correct interpretation of literature *Front. Phys.* **7** 248
[137] Miyaguchi T, Akimoto T and Yamamoto E 2016 Langevin equation with fluctuating diffusivity: a two-state model *Phys. Rev.* E **94** 012109
[138] Akimoto T and Yamamoto E 2016 Distributional behavior of diffusion coefficients obtained by single trajectories in annealed transit time model *J. Stat. Mech.* **123201**
[139] Cherstvy A G and Metzler R 2016 Anomalous diffusion in time-fluctuating non-stationary diffusivity landscapes *Phys. Chem. Chem. Phys.* **18** 23840
[140] Sposini V, Chechkin A V, Seno F, Pagnini G and Metzler R 2018 Random diffusivity from stochastic equations: comparison of two models for Brownian yet non-Gaussian diffusion *New J. Phys.* **20** 043044
[141] Sposini V, Chechkin A V and Metzler R 2018 First passage statistics for diffusing diffusivity *J. Phys.* A **52** 04LT01

[142] Thapa S, Lomholt M A, Krog J, Cherstvy A G and Metzler R 2018 Bayesian nested-sampling analysis of single-particle tracking data: maximum likelihood for the models of stochastic diffusivity and fractional Brownian motion *Phys. Chem. Chem. Phys.* **20** 29018
[143] dos Santos M A F, Dornelas V, Colombo E H and Anteneodo C 2020 Critical patch size reduction by heterogeneous diffusion *Phys. Rev.* E **102** 042139
[144] Yuste S B, Abad E and Escudero C 2016 Diffusion in an expanding medium: Fokker-Planck equation, Green's function and first-passage properties *Phys. Rev.* E **94** 032118
[145] Le Vot F, Yuste S B and Abad E 2019 Standard and fractional Ornstein-Uhlenbeck process on a growing domain *Phys. Rev.* E **100** 012142
[146] Chubynsky M V and Slater G W 2014 Diffusing diffusivity: a model for anomalous, yet Brownian, diffusion *Phys. Rev. Lett.* **113** 098302
[147] Uneyama T, Miyaguchi T and Akimoto T 2015 Fluctuation analysis of time-averaged mean-square displacement for the Langevin equation with time-dependent and fluctuating diffusivity *Phys. Rev.* E **92** 032140
[148] Chechkin A V, Seno F, Metzler R and Sokolov I M 2017 Brownian yet non-Gaussian diffusion: from superstatistics to subordination of diffusing diffusivities *Phys. Rev.* X **7** 021002
[149] Jain R and Sebastian K L 2017 Lévy flight with absorption: a model for diffusing diffusivity with long tails *Phys. Rev.* E **95** 032135
[150] Miyaguchi T, Uneyama T and Akimoto T 2019 Brownian motion with alternately fluctuating diffusivity: stretched-exponential and power-law relaxation *Phys. Rev.* E **100** 012116
[151] Zhokh A A and Strizhak P E 2020 Investigation of the time-dependent transitions between the time-fractional and standard diffusion in a hierarchical porous material *Transp. Porous Media* **133** 497
[152] Wang W, Cherstvy A G, Chechkin A V, Thapa S, Seno F, Liu X and Metzler R 2020 Fractional Brownian motion with random diffusivity: emerging residual nonergodicity below the correlation time *J. Phys.* A **53** 474001
[153] Qian H, Sheetz M P and Elson E L 1991 Single particle tracking: analysis of diffusion and flow in two-dimensional systems *Biophys. J.* **60** 910
[154] Manzo C and Garcia-Parajo M F 2015 A review of progress in single particle tracking: from methods to biophysical insights *Rep. Prog. Phys.* **78** 124601
[155] Shen H, Tauzin L J, Baiyasi R, Wang W, Moringo N, Shuan B and Landes C F 2017 Single particle tracking: from theory to biophysical applications *Chem. Rev.* **117** 7331
[156] Liu S-L, Wang Z-G, Xie H-Y, Liu A-A, Lamb D C and Pang D-W 2020 Single-virus tracking: from imaging methodologies to virological applications *Chem. Rev.* **120** 1936
[157] Burnecki K, Kepten E, Garini Y, Sikora G and Weron A 2015 Estimating the anomalous diffusion exponent for single particle tracking data with measurement errors — an alternative approach *Sci. Rep.* **5** 11306
[158] Carnaffan S and Kawai R 2019 Optimal statistical inference for subdiffusion processes *J. Phys.* A **52** 135001
[159] Munoz-Gil G, Garcia-March M A, Manzo C, Martin-Guerrero J D and Lewenstein M 2020 Single trajectory characterization via machine learning *New J. Phys.* **22** 013010
[160] Krapf D *et al* 2019 Spectral content of a single non-Brownian trajectory *Phys. Rev.* X **9** 011019
[161] Robson A, Burrage K and Leake M C 2013 Inferring diffusion in single live cells at the single-molecule level *Phil. Trans. R. Soc.* B **368** 20120029
[162] Bo S, Schmidt F, Eichhorn R and Volpe G 2019 Measurement of anomalous diffusion using recurrent neural networks *Phys. Rev.* E **100** 010102(R)
[163] Serov A S, Laurent F, Floderer C, Perronet K, Favard C, Muriaux D, Vestergaard C L and Masson J-B 2020 Statistical tests for force inference in heterogeneous environments *Sci. Rep.* **10** 3783
[164] Kosztolowicz T 2019 Model of anomalous diffusion-absorption process in a system consisting of two different media separated by a thin membrane *Phys. Rev.* E **99** 022127
[165] Woringer M, Izeddin I, Favard C and Berry H 2020 Anomalous subdiffusion in living sells: bridging the gap between experiments and realistic models through collaborative challenges *Front. Phys.* **8** 134
[166] Granik N, Weiss L E, Shalom M, Chein M, Perlson E, Roichman Y and Shechtman Y 2019 Single particle diffusion characterization by deep learning *Biophys. J.* **117** 185
[167] Gan J, Liu P and Chakrabarty R K 2020 Deep learning enabled Lagrangian particle trajectory simulation *J. Aerosol Sci.* **139** 105468
[168] Kowalek P, Loch-Olszewska H and Szwabinski J 2019 Classification of diffusion modes in single-particle tracking data: feature-based versus deep-learning approach *Phys. Rev.* E **100** 032410
[169] Arts M, Smal I, Paul M W, Wyman C and Meijering E 2019 Particle mobility analysis using deep learning and the moment scaling spectrum *Sci. Rep.* **9** 17160
[170] Janczura J, Kowalek P, Loch-Olszewska H, Szwabinski J and Weron A 2020 Classification of particle trajectories in living cells: machine learning versus statistical testing hypothesis for fractional anomalous diffusion *Phys. Rev.* E **102** 032402
[171] Cichos F, Gustavsson K, Mehlig B and Volpe G 2020 Machine learning for active matter *Nat. Mach. Intell.* **2** 94
[172] Weron A, Burnecki K, Akin E J, Sole L, Balcerek M, Tamkun M M and Krapf D 2017 Ergodicity breaking on the neuronal surface emerges from random switching between diffusive states *Sci. Rep.* **7** 5404
[173] Sikora G, Wylomanska A, Gajda J, Sole L, Akin E J, Tamkun M M and Krapf D 2017 Elucidating distinct ion channel populations on the surface of hippocampal neurons via single-particle tracking recurrence analysis *Phys. Rev.* E **96** 062404
[174] Sato Y and Klages R 2019 Anomalous diffusion in random dynamical systems *Phys. Rev. Lett.* **122** 174101
[175] Yu J 2016 Single-molecule studies in live cells *Ann. Rev. Phys. Chem.* **67** 565
[176] Michalet X and Berglund A J 2012 Optimal diffusion coefficient estimation in single-particle tracking *Phys. Rev.* E **85** 061916
[177] Martin D S, Forstner M B and Käs J A 2002 Apparent subdiffusion inherent to single particle tracking *Biophys. J.* **83** 2109
[178] Backlund M P, Joyner R and Moerner W E 2015 Chromosomal locus tracking with proper accounting of static and dynamic errors *Phys. Rev.* E **91** 062716
[179] Sikora G, Kepten E, Weron A, Balcereka M and Burnecki K 2017 An efficient algorithm for extracting the magnitude of the measurement error for fractional dynamics *Phys. Chem. Chem. Phys.* **19** 26566
[180] Weiss M 2019 Resampling single-particle tracking data eliminates localization errors and reveals proper diffusion anomalies *Phys. Rev.* E **100** 042125
[181] Kerkhoff Y and Block S 2020 Analysis and refinement of 2D single-particle tracking experiments *Biointerphases* **15** 021201

[182] Ling Y, Lysy M, Seim I, Newby J M, Hill D B, Cribb J, and Forest M G 2019 Measurement error correction in particle tracking microrheology (arXiv:1911.06451)
[183] Li M, Sentissi O, Azzini S, Schnoering G, Canaguier-Durand A and Genet C 2019 Subfemtonewton force fields measured with ergodic Brownian ensembles *Phys. Rev.* A **100** 063816
[184] Sinai Y G 1970 Dynamical systems with elastic reflections. Ergodic properties of dispersing billiards *Russian Math. Surveys* **25** 137
[185] Lebowitz J L and Penrose O 1973 Modern ergodic theory *Phys. Today* **26** 23
[186] Bouchaud J-P 1992 Weak ergodicity breaking and aging in disordered systems *J. Phys.* I **2** 1705
[187] Burov S, Metzler R and Barkai E 2010 Aging and nonergodicity beyond the Khinchin theorem *Proc. Natl. Acad. Sci. USA* **107** 13228
[188] Magdziarz M and Weron A 2011 Ergodic properties of anomalous diffusion processes *Ann. Phys.* **326** 2431
[189] Moore C C 2015 Ergodic theorem, ergodic theory and statistical mechanics *Proc. Natl. Acad. Sci. USA* **112** 1907
[190] Wang X and Pleimling M 2019 Online gambling of pure chance: wager distribution, risk attitude and anomalous diffusion *Sci. Rep.* **9** 14712
[191] Mangalam M and Kelty-Stephen D G 2020 Point estimates, Simpson's paradox and nonergodicity in biological sciences (arXiv:2009.00756)
[192] Lomholt M A, Lizana L, Metzler R and Ambjörnsson T 2013 Microscopic origin of the logarithmic time evolution of aging processes in complex systems *Phys. Rev. Lett.* **110** 208301
[193] Stefani F, Hoogenboom J and Barkai E 2009 Beyond quantum jumps: blinking nanoscale light emitters *Phys. Today* **62** 34
[194] Thirumalai D, Mountain R D and Kirkpatrick T R 1989 Ergodic behavior in supercooled liquids and in glasses *Phys. Rev.* A **39** 3563
[195] Mountain R D and Thirumalai D 1989 Measures of effective ergodic convergence in liquids *J. Phys. Chem.* **93** 6975
[196] Thirumalai D and Mountain R D 1990 Ergodic convergence properties of supercooled liquids and glasses *Phys. Rev.* A **42** 4574
[197] Rytov S M, Kravtsov Y A and Tatarskii V I 1987 *Principles of Statistical Radiophysics 1: Elements of Random Process Theory* (Heidelberg: Springer)
[198] Palmer R G 1982 Broken ergodicity *Adv. Phys.* **31** 669
[199] Liang Y, Wang S, Chen W, Zhou Z and Magin R L 2019 A survey of models of ultraslow diffusion in heterogeneous materials *ASME Appl. Mech. Rev.* **71** 040802
[200] Cherstvy A G, Thapa S, Mardoukhi Y, Chechkin A V and Metzler R 2018 Time averages and their statistical variation for the Ornstein-Uhlenbeck process: role of initial particle conditions and relaxation to stationarity *Phys. Rev.* E **98** 022134
[201] Mardoukhi Y, Chechkin A V and Metzler R 2020 Spurious ergodicity breaking in normal and fractional Ornstein-Uhlenbeck process *New J. Phys.* **22** 073012
[202] Cherstvy A G, Vinod D, Aghion E, Chechkin A V and Metzler R 2017 Time averaging, ageing and delay analysis of financial time series *New J. Phys.* **19** 063045
[203] Ritschel S, Cherstvy A G, and Metzler R 2020 Universality of delayed time-averages for historical financial time series (in preparation)
[204] Black F and Scholes M 1973 The pricing of options and corporate liabilities *J. Political Econ.* **81** 637
[205] Merton R C 1973 Theory of rational option pricing *Bell J. Econ. Manage. Sci.* **4** 141
[206] Mitra P P, Sen P N, Schwartz L M and Le Doussal P 1992 Diffusion propagator as a probe of the structure of porous media *Phys. Rev. Lett.* **68** 3555
[207] Fieremans E, Novikov D S, Jensen J H and Helpern J A 2010 Monte Carlo study of a two-compartment exchange model of diffusion *NMR Biomed.* **23** 711
[208] Kärger J 1985 NMR self-diffusion studies in heterogeneous systems *Adv. Coll. Interf. Sci.* **23** 129
[209] Novikov D S 2020 personal communication
[210] Novikov D S, Fieremans E, Jensen J H and Helpern J A 2011 Random walks with barriers *Nat. Phys.* **7** 508
[211] Perge J A, Niven J E, Mugnaini E, Balasubramanian V and Sterling P 2012 Why do axons differ in caliber? *J. Neurosci.* **32** 626